Shifts in organic matter character and microbial assemblages from glacial headwaters to downstream reaches in the Canadian Rocky Mountains

Hayley F. Drapeau[1,2], Suzanne E. Tank[1], Maria A. Cavaco[2], Jessica A. Serbu[1], Vincent L. St. Louis[1], Maya P. Bhatia[2,3]

[1]Department of Biological Sciences, University of Alberta, Edmonton, T6G 2R3, Canada
[2]Department of Earth and Atmospheric Sciences, University of Alberta, Edmonton, T6G 2R3, Canada
[3]Deceased
Correspondence to: Suzanne Tank (suzanne.tank@ualberta.ca)

Abstract. Climate change is causing mountain glacial systems to warm rapidly, leading to increased water fluxes and concomitant export of glacially-derived sediment and organic matter (OM). Glacial OM represents an aged, but potentially bioavailable carbon pool that is compositionally distinct from OM found in non-glacially sourced waters. Despite this, the composition of riverine OM from glacial headwaters to downstream reaches and its possible role in structuring microbial assemblages have rarely been characterized in the Canadian Rockies. Over three summers (2019–2021) we collected samples before, during, and after glacial ice melt along stream transects ranging 0 – 100 km downstream of glacial termini on the eastern slopes of the Canadian Rocky Mountains. We quantified dissolved and particulate organic carbon (DOC, POC) concentration, and used isotopes (Δ^{14}C-OC, δ^{13}C-OC) and dissolved OM (DOM) absorbance and fluorescence to assess OM age, source, and character. Environmental data were combined with microbial 16S rRNA gene sequencing to assess controls on the composition of stream_water microbial assemblages. From glacial headwaters to downstream reaches, OM showed a clear transition from being aged and protein-like with an apparent microbial source to being relatively younger and humic-like. Indicator microbial species for headwater sites included chemolithoautotrophs and taxa known to harbour adaptations to cold temperatures and nutrient-poor conditions, suggesting some role for glacial seeding of microbial taxa to headwaters of this connected riverine gradient. However, physical and chemical conditions (including water temperature; POC concentration; protein-like DOM; and deuterium excess, an additional indicator of water source) could only significantly explain ~9% of the observed variation in microbial assemblage structure. This finding, paired with the identification of a ubiquitous core microbial assemblage that comprised a small proportion of all identified amplicon sequence variants (ASVs), but was present in large relative abundance at all sites, suggests that mass effects (i.e., whereby high dispersal rates causes homogenization of adjacent communities) largely overcome species sorting to enable a connected microbial assemblage along this strong environmental gradient. Our findings suggest that a loss of novel glacial and microbial inputs with climate change, coupled with catchment terrestrialization, could change OC cycling and microbial assemblage structure across the evolving mountain-to-downstream continuum in glacierized systems.

1 Introduction

Anthropogenic climate change is causing glaciers to retreat at unprecedented rates (Zemp et al., 2015). Rapid glacial retreat has the potential to impact downstream hydrology (Clarke et al., 2015), carbon cycling (Hood et al., 2015; Hood et al., 2020) and microbial assemblage dynamics (Bourquin et al., 2022; Hotaling et al., 2017), as source water contributions to headwater streams undergo fundamental change. In the Canadian Rocky Mountains, glacial meltwater contributions to downstream rivers is presently increasing but is projected to peak by 2040 (Clarke et al., 2015; Pradhananga and Pomeroy, 2022). Over the coming decades, the eventual disappearance of glacial meltwater additions to glacially-fed rivers is predicted to lead to decreased summer flows and water availability, impacting millions of individuals in communities downstream (Anderson and Radić, 2020).

Changing contributions of glacial meltwater to headwater streams could disrupt downstream riverine carbon dynamics, because glaciers provide, and internally cycle, unique sources of organic carbon (OC) (Hood et al., 2015; Musilova et al., 2017; Wadham et al., 2019). As glaciers melt, the formation of supra- and sub-glacial channels can cause meltwater to be routed on top of, through, and/or underneath, glaciers (Nienow et al., 1998). At the beginning of the melt season, water is typically sourced from snowmelt which is inefficiently routed through a distributed hydrological network at the ice–bed interface or along the ice margin, and is characterized by high rock:water contact times (Arendt et al., 2016). As the melt season progresses an efficient subglacial network forms facilitating rapid transit through the subglacial environment (Arendt et al., 2016) or routing of water laterally via marginal streams. This meltwater is then exported into headwater streams where it provides an important seasonal control on stream hydrology via augmentation of summer discharge (Campbell et al., 1995), and biogeochemistry via its unique chemical signature (Milner et al., 2017). The contribution of glacially sourced water to headwater streams enables movement of novel organic matter (OM) from overridden vegetation at the glacier bed (Bhatia et al., 2010), anthropogenic aerosols on the ice surface (Stubbins et al., 2012), and *in situ* microbial ~~communities~~ assemblages (Stibal et al., 2012) to downstream systems. Previous studies have shown that glacially derived dissolved OM (DOM) is aged (Bhatia et al., 2013; Hood et al., 2009; Stubbins et al., 2012), exhibits protein-like fluorescence (Barker et al., 2009; Kellerman et al., 2020), and can serve as a labile substrate for downstream microorganisms (Hood et al., 2009; Singer et al., 2012). In contrast, glacially derived particulate OM (POM, and its OC subset POC), which has been less studied, can be predominantly derived from comminuted rock and sediment, and can persist within rivers (Cui et al., 2016, Hood et al., 2020). During transit through fluvial networks, glacially exported OM mixes with non-glacial terrestrially derived OM, which typically exhibits a humic-like fluorescent signature (McKnight et al., 2001a), is relatively younger (Raymond and Bauer, 2001), and has generally been shown to be less accessible for microbial consumption (D'Andrilli et al., 2015).

River ecosystems are overwhelmingly heterotrophic, with food webs sustained by microbial consumption and mineralization of OM inputs (Bernhardt et al., 2022). OM composition has been found to be an important determinant of microbial assemblage

Formatted: Font: Italic

65 structure (Judd et al., 2006) alongside environmental factors such as light, river flow regimes (Bernhardt et al., 2022; Milner et al., 2017), temperature, and nutrient availability (Elser et al., 2020). Thus, the increase and eventual decline of glacial meltwater inputs to fluvial networks, with their entrained glacial OM, may impact microbial assemblages. In addition, headwater assemblages can shift as a result of the direct loss of novel glacially-sourced microbes (Wilhelm et al., 2013) as glaciers have been found to host unique microbial taxa in both the supraglacial and subglacial environments (Bourquin et al.,

70 2022; Hotaling et al., 2017; Stibal et al., 2012). These taxa are often uniquely adapted to glacial conditions, such as seasonally fluctuating and overall low nutrient concentrations, cold temperatures, and the presence of reduced chemical species in low oxygen subglacial environments, which can select for chemosynthetic metabolisms (Bourquin et al., 2022; Hotaling et al., 2017). Recent work at European, Greenlandic, and North American glaciers indicates that microbes from supraglacial environments are readily entrained in meltwaters, enabling these flow paths to seed downstream microbial ~~communities~~

75 assemblages (Stevens et al., 2022). Overall, if changes in glacial loss drive changes in microbial assemblage composition, this could lead to a loss of unique metabolic pathways (Bourquin et al., 2022), changes in respiratory efflux of CO_2 (e.g., Singer et al., 2012), and food web perturbations, given that OM incorporated into microbial biomass is assimilated by higher trophic level organisms (e.g., Fellman et al., 2015).

80 In this study, we pair measurements of stream OM and microbial assemblage composition along transects from glacial headwaters to downstream reaches, with sampling across three years and encompassing conditions prior to, during, and after the summer glacial melt season. We undertake this work in glacially-fed fluvial networks draining eastward from the Canadian Rocky Mountains, to assess how glacial loss will impact downstream microbial diversity and carbon cycling in this region. The icefields (Wapta and Columbia) that feed these alpine glaciers are rapidly shrinking and are projected to be reduced by

85 80–100% of their 2005 area by 2100 (Clarke et al., 2015). Our objectives in this rapidly changing landscape were three-fold: first, to investigate spatial and temporal variation in stream OM age, source, and character across different hydrological periods in three Rocky Mountain rivers with a distance ranging from 0–100 km downstream from glacial termini; second, to characterize microbial assemblage composition and its variation along this same gradient; and finally, to identify environmental drivers of variation in microbial assemblage structure, with a particular focus on OM composition. We

90 hypothesized that: (1) OM character, apparent source, and age would transition along our 100 km transects; (2) microbial assemblages would similarly vary along our transects; and (3) these shifts would be tied, such that changes in OM and other chemical parameters would structure microbial assemblages from headwaters to downstream reaches.

2 Methods

2.1 Site description

95 Samples were collected from the Sunwapta-Athabasca, North Saskatchewan (NSR) and Bow rivers located within Banff and Jasper National Parks of the Canadian Rocky Mountains (Fig. 1). Each of these rivers are sourced from glacial headwaters with the Sunwapta-Athabasca and NSR receiving inputs predominately from the Columbia Icefield, and the Bow River receiving inputs from the Wapta Icefield. At ~216 km^2 (Tennant and Menounos, 2013; Bolch et al., 2010), the Columbia Icefield is the largest icefield in the Canadian Rockies, while the Wapta Icefield is smaller at ~80 km^2 (Ommanney, 2002).

100

Along each river we chose three to four sampling sites at which we examined how stream OM and microbial characteristics transitioned with increasing distance from glacial input. Sampling sites ranged from glacial headwaters (0 km downstream of glacial inflow) to 100 km downstream of glacial termini. For certain statistical analyses (predominantly, associated with microbial assemblage structure), sites were binned into four distance ranges, ~~selected a priori~~ based on variation in the upstream

105 catchment between sites: headwater (0.2 km downstream), near (2–6 km downstream), mid (18–50 km downstream) and far (>50 km downstream) (Fig. 1a). These bins were selected *a priori*, to enable a gradient of sites within each sampled river, and based on variation in the upstream catchment between sites (Table S1). For example, the "headwater" site had no catchment forest cover, "near" sites ranged from 0.3 – 5% forest and 42-55% snow and ice, and "far" sites had greater than 25% forest, and 6-12% snow and ice (Table S1). Sites were restricted to locations within Banff and Jasper National Parks to enable a

110 comparison of study sites that were minimally impacted by direct anthropogenic landscape disturbance. Throughout, we generally use "stream" to refer to specific sites, although we acknowledge that our transects span from glacial headwaters to relatively large riverine reaches.

Samples were collected over a three-year study period (Fig. 1b). Each of the sample sites were visited every three to four weeks

115 throughout the months of May to October during 2019, 2020, and 2021. Opportunistic samples were also collected at a subset of sites in December 2019 and January 2021. This sampling design enabled us to cover the three main hydrological stages in a glacially sourced river: prior to the seasonal glacial ice melt (pre-melt; n=2 visits, 24 samples total), the glacial melt period (melt; n=13 visits, 177 samples), the post-glacial ice melt period (post-melt; n=1 visit, 14 samples), and during winter (n=2 visits; 7 samples). Hydrological periods were determined using the Environment and Climate Change Canada (ECCC) stream

120 discharge hydrographs from Athabasca Glacier (station ID: 07AA007) (ECCC, 2022) (Fig. 1b). We defined the pre-melt stage as the period when monthly average stream discharge at the Athabasca glacier headwater was low (< 1 m^3 s^{-1}; assessed as the inflection point on the Athabasca Glacier hydrograph); a likely indication that glacial meltwater channels were not yet established (Arendt., 2015). The glacial melt period was defined as the period when monthly average discharge was high (>1, but rapidly transitioning to >2.5 m^3 s^{-1}; discharge typically peaked during July–August); at this time glacial meltwater channels

4

Formatted: Font: Italic

125 were likely well established, with melting glacier ice contributing substantially to headwater stream flow. Finally, the post-melt period was characterized by, once again, low average monthly discharge at the glacier headwater (< 1 m^3 s^{-1}; typically, October and onwards); likely indicating closed glacial channels and cessation of ice melt input. In 2019, all three hydrological stages (pre-melt, melt, post-melt) were sampled; in 2020, sampling was delayed due to the COVID-19 pandemic, and samples were only collected during the melt and post-melt stages; in 2021, samples were collected during the pre-melt and melt stages

130 only. Over our three-year study period, 2019 exhibited the lowest melt-period discharge and 2021 the highest (Fig. 1b).

2.2 Field sampling and field laboratory processing

At each site samples were collected for: DOM absorbance and fluorescence, DOC concentration, POC concentration, particulate and dissolved OC isotopes (δ^{13}C-DOC, δ^{13}C-POC, Δ^{14}C-DOC, Δ^{14}C-POC), and 16S rRNA gene sequencing. To further assess water source and hydrochemical controls on microbial diversity in our analyses, we used data for water

135 isotopes (δ^{18}O-H$_2$O, δ^2H-H$_2$O), nutrients (ammonia (NH$_4^+$), nitrate and nitrite (NO$_3^-$+NO$_2^-$), total dissolved nitrogen (TDN), total nitrogen (TN), soluble reactive phosphorous (SRP), total dissolved phosphorus (TDP), total phosphorous (TP), and dissolved silica (SiO$_2$)), major anions and cations (Mg^{2+}, Cl$^-$, Na^{2+}, SO$_4^{2-}$, Ca^{2+}, K$^+$), trace metals (Al^{3+}, Ba^{2+}, dCr, dMn, dMo, dNi, Sr^{2+}), temperature, and specific conductance that were collected at each trip (see also Serbu et al. 2024). All sample bottles, except those for anions and nutrients, were soaked overnight in a dilute acid bath (1.2 mol L^{-1} trace metal

140 grade HCl), rinsed at least 3 times with 18.2 MΩ MilliQ water, and rinsed three times with sample water before collection at the field site. Bottles for anion and nutrient analyses were new, following the tested protocol in the CALA (Canadian Association for Laboratory Accreditation) certified laboratory where these analyses were run (University of Alberta Biogeochemical Analytical Services Laboratory; BASL). Trace metal bottles were pre-soaked in a 0.01% Citranox (phosphate free detergent) bath prior to the acid bath step. Following the HCl soak and MilliQ water rinse, all glassware

145 (bottles, EPA vials, and filtration apparatus) were combusted at 560°C for a minimum of 4 h, and high-density polycarbonate (HDPC) bottles for microbial analysis were autoclaved. Glass microfibre filters (grade GF/F, Whatman) were combusted at 460°C for a minimum of 4 h prior to use. High-density polyethylene (HDPE) bottles for ion collection were pre-washed with Citranox prior to the acid cleaning procedure.

150 Samples for DOM absorbance and fluorescence, DOC concentration and δ^{13}C-DOC were sub-sampled from a 250 mL amber glass collection bottle and filtered streamside through 0.45 µm polyethersulfone (PES) filters (Fisherbrand Basix; pre-rinsed with 60 mL Milli-Q and 15 mL river water) into combusted 40 mL amber EPA vials. Nutrient samples were sub-sampled from a 500 mL HDPE collection bottle and filtered streamside using a pre-rinsed sterile plastic syringe and a pre-rinsed 0.45 µm cellulose acetate filter (Sartorius) into polypropylene collection bottles. Water isotope samples were filtered streamside using

155 either 0.45 µm cellulose acetate (in 2019, 2020) or PES (in 2021) filters into 2mL glass (2019, 2020) or 25mL HDPE scintillation (2021) vials filled with no headspace. Major ions and trace metals were sub-sampled from a 250 mL HDPE

5

collection bottle and filtered streamside into 20 mL scintillation vials using rubber free syringes and a 0.45 μm PES filter. Water temperature and specific conductance were measured onsite using a YSI EXO sonde. Bulk water samples were collected for microbial assemblage analyses in prepared (see above) HDPC bottles, radiocarbon (Δ^{14}C-DOC, Δ^{14}C-POC) in Teflon bottles, and POC concentration and δ^{13}C-POC samples in 4L HDPE plastic bottles. All bulk water chemistry samples (for Δ^{14}C-DOC, POC concentration, Δ^{14}C-POC, and δ^{13}C-POC) were filtered within 24 h of collection off site. Samples for 16S rRNA gene sequencing were generally filtered within 4–12 h of collection, apart from the Bow River samples that were filtered after 24 h of collection. To minimize the effects of differential processing times on assessing microbial assemblage dynamics, Bow River samples were excluded from our microbial analysis but retained in the hydrochemical and carbon analyses.

Two litre bulk water samples collected for 16S rRNA gene sequencing were filtered "until refusal" using a 0.22 μm Sterivex (MilliporeSigma) filter and a peristaltic pump operated at 50–60 mL min^{-1} to minimize cell breakage. A field blank, consisting of a clean 2L polycarbonate bottle filled with milliQ water, left opened at each site, was also processed in the same way to control for any outside contamination during processing. Dissolved radiocarbon samples were filtered through a 0.7 μm GF/F filter using a glass filter tower, collected into 1L amber glass bottles, and acidified to pH 2 using HPLC grade H$_3$PO$_4$. Material retained on the 0.7 μm GF/F filter was used for Δ^{14}C-POC analysis. Samples for POC concentration and δ^{13}C-POC were collected on 0.7 μm GF/F filters using plastic filter towers. Samples for DOC concentration and δ^{13}C-DOC were acidified to pH 2 using trace metal grade HCl. Cation and trace metal samples were acidified to pH 2 using trace metal grade HNO$_3$. Samples for DOC concentration, δ^{13}C-DOC, Δ^{14}C-DOC, DOM absorbance and fluorescence, anions, TDN, TDP and dSi were stored at 4°C; samples for NH$_4^+$, NO$_3^-$+NO$_2^-$, δ^{13}C-POC, Δ^{14}C-POC were stored at -20°C, and sterivex filters were flash frozen in a liquid nitrogen dry shipper and upon return to the laboratory stored at -80°C until analysis.

2.3 Laboratory analyses

2.3.1 DOM absorbance and fluorescence, DOC, POC and OC isotopes

DOM absorbance and fluorescence were analysed using a HORIBA Scientific Aqualog with a 1 cm path length quartz cuvette. Absorbance scans were collected over a 240–800 nm wavelength range in 1 nm increments with a 0.5 s integration time. Excitation emission matrices (EEMs) were constructed over a 230–500 nm excitation wavelength range with an increment of 5 nm and a 5 s integration time, with an emission coverage increment of 2.33 nm with a 230–500 nm emission wavelength range.

DOC samples were analysed using a Shimadzu Total Organic Carbon analyser. Samples with less than 1 mg L^{-1} DOC were analysed on a Shimadzu TOC-V equipped with a high sensitivity catalyst, using a 2 mL injection and five minute sparge time. Samples estimated (from absorbance) to have more than 1 mg L^{-1} DOC were analysed using a Shimadzu TOC-L fitted with a

regular sensitivity catalyst, using a 150 μL injection and five minute sparge time. For analyses on the TOC-V, a five point (0-1 mg L^{-1}) or six point (0-0.5 mg L^{-1}) calibration curve (R^2 > 0.98) was created daily using dilution from a 5 mg L^{-1} stock solution (SCP Science). For analyses on the TOC-L, a five point (0-1 mg L^{-1} or 0-2 mg L^{-1}) calibration curve (R^2 > 0.98) was created through dilution of either 5 mg L^{-1} stock solution (SCP Science) or a 10 mg L^{-1} stock solution (SCP Science). Reference waters were created using dilution of a 5 mg L^{-1} stock solution (SCP Science) or from a 1 mg C L^{-1} caffeine solution. Reference waters and MilliQ blanks were run every ten samples and were within 10% of accepted values. Samples were blank corrected via the subtraction of mean blank concentrations of MilliQ samples run prior to ten sample groups to account for instrument drift.

POC, δ^{13}C-POC and Δ^{14}C-POC samples were subjected to a heated acid fumigation following procedures outlined in Whiteside et al. (2011). Briefly, this involved heating the filters at 60°C for 24 h in a desiccator with 20 mL of concentrated trace metal grade HCl, then neutralizing the filters at room temperature for 24 h in a desiccator with NaOH pellets. Samples for POC concentration and δ^{13}C-POC were packaged into tin capsules before being measured using an Elementar VarioEL Cube Elemental Analyser a DeltaPlus Advantage isotope ratio mass spectrometer with a ConFlo III interface (δ^{13}C-POC only) at the Environmental Isotope Laboratory at the University of Waterloo (in 2019) or the Jan Veizer Stable Isotope Laboratory (Ottawa, ON, Canada, in 2020 and 2021). δ^{13}C-DOC samples were analysed using the wet oxidation method on an OI Analytical Aurora model 1030 wet TOC analyzer connected to an Isotope Ratio Mass Spectrometer (IRMS) at the Jan Veizer Stable Isotope Laboratory. Δ^{14}C-POC samples were processed via organic combustion and Δ^{14}C-DOC samples were processed using UV-oxidation, prior to graphitization and accelerator mass spectrometry analysis at the André E. Lalonde AMS Laboratory at the University of Ottawa (in 2019) or the National Ocean Sciences Accelerator Mass Spectrometry laboratory (NOSAMS; WHOI, Woods Hole, MA, USA, in 2020 and 2021; Batch numbers = 67580, 67380, 67069, 66828).

2.3.2 Hydrochemical samples

Nutrient (NH$_4^+$, NO$_3^-$+NO$_2^-$, TDN, TDP, TN, TP, dSi, SRP), trace metal (Al^{3+}, Ba^{2+}, dCr, dMn, dMo, dNi, Sr^{2+}), and ion (Mg^{2+}, Cl$^-$, Na$^+$, SO$_4^{2-}$, Ca^{2+}, K$^+$) samples were analysed at the CALA accredited BASL facility at the University of Alberta (Edmonton, AB, Canada) (see Table S2 for detection limits and method details). Nutrient samples were analysed using flow injection analysis on a Lachat QuikChem 8500 FIA automated ion analyser and anions were analysed via ion chromatography on a Dionex DX600. Cations and trace metals were analysed using Inductively Coupled Plasma-Mass Spectrometry, on a Thermo Scientific iCAP Q (2019) and Agilent 7900 (2020-21). Water isotopes (δ^{18}O-H$_2$O and δ^2H-H$_2$O) were analysed using a Picarro L2130 isotope and gas concentration analyser calibrated using standard references obtained from ice core water (USGS46) and Lake Louise drinking water (USGS47) (United States Geological Survey). Reference waters and MilliQ were run every 20 samples and were within 20% of accepted values. Sample values were calculated from an average of three injections where the standard deviation of δ^{18}O-H$_2$O was less than 0.2 and the standard deviation for δ^2H-H$_2$O was less than

220 1; the first five injections were typically excluded due to memory effects. δ^{18}O-H$_2$O and δ^2H-H$_2$O were used to calculate deuterium excess, which we use as an indicator of water source given its known increase with elevation, and therefore water sourced from glaciers and high elevation snow (Bershaw et al., 2019; Bershaw et al., 2020; Boral et al., 2019)

2.3.3 Lab and bioinformatic processing of microbial samples

Bulk genomic DNA collected on the Sterivex filter was extracted using a DNeasy PowerWater Sterivex kit (Qiagen) according
225 to the manufacturer's instructions (Qiagen, 2019) with an amendment of a 1 h at 72°C for the initial incubation time, rather than 90°C for 5 mins, to increase DNA yield. Measured genomic DNA extracted from filters ranged from below detection (<0.5 ng µL^{-1}) to 20.8 ng µL^{-1}; when DNA concentrations quantified below 10 ng µL^{-1} on the Qubit following DNA extraction, we added 5uL of template DNA (default is 2.5uL), along with bovine serum albumin (BSA) to maximize DNA available for PCR, adjusting for total water added to the reaction.
230
Extracted samples, including field blank samples and a separate negative control containing PCR grade water as template, were amplified using the 515F (5'GTGYCAGCMGCCGCGGTAA'3) and 926R (5'CCGYCAATTYMTTTRAGTTT'3) primers (Parada et al., 2016) targeting the V4–V5 hypervariable region of the 16S rRNA gene with the following protocol: 3 min initial denaturation at 98°C, 35 cycles of: 30 s denaturation, 30 s primer annealing at ~ 60°C and 30 s extension at 72°C;
235 and finally, 10 mins of final extension at 72°C. Polymerase Chain Reaction (PCR) products were visualized on a 1.5% agarose gel. Any samples showing a band at the expected size of ~400bp and those samples showing product on the gel were subsequently purified using Nucleomag beads (ThermoFisher Scientific) at a 0.8 ratio of beads: sample. The purified samples were then indexed, using unique indexes that were added to each sample using i7 and i5 adapters (Illumina) to construct the final library. These indexed samples underwent another purification using the same Nucleomag bead procedure outlined above.
240 These purified, indexed samples, representing each year of sampling (2019, 2020, 2021) were then pooled together at 5 µL each, where fainter samples were added at 10 µL. We only purified and pooled samples if our negative control did not amplify (no band on the gel), demonstrating no introduction of exogenous contamination during library preparation steps. Unique indexes were then added to each sample using i7 and i5 adapters (Illumina) to construct the subsequent library. All amplicon and barcoded products from each respective year of sampling (2019, 2020, 2021) were verified on a 1.5% agarose gel and
245 those that could be successfully visualized were then pooled (12.4 ng µL^{-1}, 20.17 ng µL^{-1}, 14.3 ng µL^{-1}). The final quality of each pool was determined on an Agilent 2100 Bioanalyzer at the Molecular Biology Service Unit (University of Alberta, Edmonton, AB, Canada) using a high sensitivity DNA assay prior to submitting the library for 16S rRNA gene sequencing. The final prepared 2–4 nM libraries, containing up to 50% PhiX Control v3 (Illumina, Canada Inc., NB, Canada; see below) were sequenced on an Illumina MiSeq (Illumina Inc., CA, USA) using a 2 × 250 cycle MiSeq Reagent Kit v3 submitted at the
250 Molecular Biological Services Unit (Univ. of Alberta) in 2019 and The Applied Genomics Core (Univ. of Alberta) in 2020 and 2021. Measured genomic DNA extracted from filters ranged from below detection (<0.5 ng µL^{-1}) to 20.8 ng µL^{-1}; when

8

255

Sequence data was demultiplexed using MiSeq Reporter software (version 2.5.0.5) and Miseq Local Run Manager GenerateFastQ Analysis Module 3.0. The assembled data was then processed using the Quantitative Insights into Microbial Ecology (QIIME2) pipeline (Boylen et al., 2020, version 2021.11). Sequences were clustered into amplicon sequence variants (ASVs) with chimeric sequences and singletons removed using DADA2 (Callahan et al., 2019). All representative sequences

260 were classified with the SILVA v138 taxonomic database (Quast et al., 2013, Yilmaz et al., 2014), at the default 0.8 similarity cut-off. ASV sequences that were identified as eukaryotes or chloroplasts were removed. Samples were decontaminated by removing ASVs present in a sequenced field blank using the prevalence method with a threshold of 0.5 (Karstens et al., 2019; Parada et al., 2016b). No positive controls were included in our sequencing run, because we have spiked in with PhiX quite heavily into our pool (~50%)., which is a quality control reagent used commonly in sequencing runs to optimize cluster

265 generation, sequencing, alignment and calibration control throughout the run. Because PhiX is a well-defined bacteriophage genome, it has a diverse base composition that provides the balanced fluorescent signal that low diversity sample libraries, like ours, lack, during each sequencing cycle (Illumina). A large proportion of PhiX was therefore added to increase the diversity of our oligotrophic pool, such that the reads obtained will generally correspond with the most abundant microbial taxa in the sample, as a function of this and the read coverage of the MiSeq. Following inspection of rarefaction curves (Fig. S1), samples

270 with less than 5,000 reads were excluded from further analysis because they had not reached a plateau, indicating that sequencing might not have captured a good representation of speciesASVs.

2.4 Data analysis

2.4.1 DOM absorbance and fluorescence calculations and PARAFAC analysis

275 EEMs were corrected for inner filter effects, Raman normalized, blank corrected and had Rayleigh and Raman scatter bands removed prior to parallel factor (PARAFAC) analysis (Murphy et al., 2013). PARAFAC analysis was performed in Matlab (Version 9.12.0) using the drEEM toolbox (Version 0.6.5) (Murphy et al., 2013). PARAFAC models of up to seven components were assessed and samples with high leverage were removed. A four-component model was validated using split-half analysis and was ultimately selected based on a low sum of square error and visual confirmation that only random noise

280 remained in the residuals. Absorbance scans were utilized to calculate specific UV absorbance at 254 nm ($SUVA_{254}$; a measure of DOM aromaticity) (Weishaar et al., 2003) and the spectral slope coefficient between 275 and 295 nm ($S_{275-295}$; a measure of DOM molecular weight) (Helms et al., 2008). Corrected fluorescence data were utilized to calculate the fluorescence index (FI) (McKnight et al., 2001b), humification index (HIX) and biological index (BIX) (Huguet et al., 2008), and the proportional

9

contribution of common fluorescence peaks (peaks A, B, C, M, T; (Coble, 1996)). Further description of absorbance and
285 fluorescence-based metrics is provided in Table S3.

2.4.2 Geochemistry

We ran linear mixed-effects models with distance (as km downstream) and season (comparing winter, pre-melt, melt, and post-
melt) as fixed effects, and river and year as random effects, to explore variation in geochemical parameters (OC concentration,
OM character, OC isotopic composition, and water isotopes). We ran a Type II ANOVA on model outputs to assess significant
290 main effects of distance and season, and their interaction. When the effect of season was significant, the analysis was followed
by Tukey-adjusted contrasts using estimated marginal means. A linear model was used to assess the relationship between
Δ^{14}C-DOC and protein-like PARAFAC components. We use deuterium excess as proxy for glacial meltwater because it is
known to increase with elevation (Bershaw et al., 2019) and is thus typically higher in glacial ice (Souchez et al., 1983) and
water contributions from high elevation snow (Bershaw et al., 2020) when compared to lower elevation (downstream) water
295 sources. To explore how DOM parameters varied across hydrologic seasons and with distance downstream a principal
component analysis (PCA) was performed. Deuterium excess was fitted onto the ordinated PCA as a passive overlay (i.e., fit
post-ordination) to not affect the analytical output, using envfit (Oksanen, 2007).

2.4.3 Microbial analyses

To enable contrasts between sites most strongly influenced by glaciers (i.e., the headwater and near sites; 42 – 55% snow and
300 ice coverage in catchment; Table S1) and those further downstream (here "far" sites, with 6 – 12% snow and ice coverage in
catchment), the mid distance range sites were excluded from statistical analysis of the microbial samples. Alpha diversity was
calculated on untransformed data using the Shannon index (Hill, 1973) and beta diversity was visualized using non-parametric
multi-dimensional scaling (NMDS), using a Bray Curtis distance matrix created from Hellinger-transformed ASV abundance
data (Ramette, 2007; Legendre and Gallagher, 2001). Significant differences between *a priori* determined clusters on the
305 NMDS were assessed using permutational multivariate ANOVAs (perMANOVA), set at 999 permutations and using the Bray
Curtis distance matrix. The clusters used for comparison included distance (headwater, ~~mid~~near, and far), year, and river. We
additionally constructed a Venn Diagram in R using packages from *dplyr* and *vegan* to explore ASV overlap between
headwater, mid, and far sites, and refer to ASVs present across all distance bins as a "core" ~~community~~assemblage, below. To
explore the possible role of environmental control on microbial assemblage structure, we performed a backward selection
310 distance based redundancy analysis (RDA) on Hellinger-transformed ASV abundance data and non-correlated normally scaled
environmental parameters. To do this, we first considered a broad suite of environmental parameters in a non-stepped RDA
including temperature, pH, specific conductance, turbidity, DOC concentration and DOM composition (% humic-like [see
Section 3.1.2], FI, BIX, HIX, peak A, peak B, peak C, peak M, peak T, $S_{275-295}$, SUVA$_{254}$), nutrients (TP, TDN, dSi), major
ions, and trace metals , and used a variance inflation factor (VIF) of 10 as a benchmark to omit highly correlated parameters

10

Formatted: Font: Italic

315 to avoid an over-parameterized model. The backward selection RDA was run on this streamlined set of parameters, and percent variance of the model output was adjusted following the approach of Peres-Neto et al. (2006). An indicator species analysis (ISA) was performed on raw (non-transformed) ASV abundance data (Dufrêne and Legendre, 1997). Indicator values were compared to the Spearman rank correlation coefficient for the relationship between ASV abundance and deuterium excess, to explore how the presence of indicator species varied across gradients of water source. We re-ran (i.e., as a check on output)

320 NMDS and perMANOVA analyses using rarefied, rather than Hellinger-transformed, datasets, to confirm the suitability of the Hellinger transformation for our analyses. Of our target sample set, we successfully obtained sequences from 72 samples, with ASV richness ranging from 81 to 9,634, and read counts ranging from 5,066 to 409,740; inspection of rarefaction curves confirms that a plateau were reached for all included samples (i.e., those with greater than 5,000 reads; Fig. S1).

325 All data were analysed within the R statistical language, using *vegan* (Oksanen, 2007), *lme4* (Bates et al. 2015), *car* (Fox and Weisberg 2019), *emmeans* (Lenth, 2024), *stardom* (Pucher et al., 2019), *decontam* (Davis et al., 2018), *indicspecies* (Cáceres and Legendre, 2009), and base packages (R Core Team, 2022). Variance adjustment within the RDA used the function "RsquareAdj", and the perMANOVA was performed using the function "adonis", both in *vegan*. Data visualization utilized the package *ggplot2* (Wickham, 2016).

330 **3 Results**

3.1 Spatial and temporal variation in stream organic matter characteristics

3.1.1 Water isotopes, DOC concentration and DOM composition

In a model with sample year and river as random effects, deuterium excess declined with distance downstream (χ^2_1=58.75; p<0.001) and varied seasonally (χ^2_3=58.75; p<0.001) with values greater during melt than pre-melt seasons (p<0.001) (Fig.

335 S1bS2b, Tables S4, S5). δ^{18}O-H_2O also varied seasonally (χ^2_3=30.81; p<0.001), becoming more enriched from pre-melt to melt (p=0.001), and melt to post-melt seasons (p < 0.023) (Fig. S1aS2a, Tables S4, S5). A two-way ANOVA to assess differences in water source between the *a priori* selected distance bins showed deuterium excess to vary significantly between bins ($F_{3,186}$ = 44.74, p<0.001), with Tukey post-hoc comparisons showing headwater and near sites to be similar to each other (p=0.15), but all other bins to be significantly different from one another (p<0.001).

340

DOC concentrations were universally low closest to the glacier (0.09–0.76 mg L^{-1}) and increased with distance downstream (χ^2_1=44.87; p<0.001) (Fig. 2a, Table S4). Concentrations also varied seasonally (χ^2_3=58.75; p<0.001), with pre-melt concentrations greater than those during melt (p<0.001), post-melt (p<0.001) and winter (p<0.001). However, a significant interaction suggests that these effects were not necessarily consistent (χ^2_3=17.06; p<0.001) (Fig. 2a, Tables S4, S5). Across all

11

345 sites and dates, POC concentrations ranged from 0.04 mg L^{-1} to 2.8 mg L^{-1}. POC was typically the dominant component of the total OC (TOC) pool at glacial headwaters (POC:TOC = 0.32–0.89; median value > 0.5 for all but pre-melt 2021; data not shown), and showed a proportional decline with distance downstream (χ^2_1=18.31; p<0.001) (Fig. 2e; Table S4).

From the suite of PARAFAC models considered, a four component model was selected (Fig. S2S3). Using the OpenFluor
350 database (Murphy et al., 2014), components 1 (C1) and 2 (C2) were identified as humic-like components, component 3 (C3) was identified as a tryptophan-like (protein-like) component, and component 4 (C4) was identified as a tyrosine-like (protein-like) component (Table S6). The proportion of protein- (sum of C3 and C4) and humic- (sum of C1 and C2) like components transitioned along transects, with humic-like DOM increasing proportionately with distance downstream, while protein-like DOM proportionally decreased (χ^2_1=43.96; p<0.001) (Fig. 2b–c, Table S4). Overall, the proportion of humic-like DOM was
355 greater in the pre-melt than melt (p=0.005) and post-melt (p<0.001) periods (Table S5).

3.1.2 Dissolved and particulate OC isotopes

δ^{13}C-DOC ranged from -35 to -20.2‰ (Figs. 3a and 4), showing a marginal enrichment with distance downstream (χ^2_1=3.57; p=0.059; Table S4), and significant variation across season (χ^2_3=9.68; p=0.022; Table S4), with depleted values during the pre-melt (p=0.050) and melt (p=0.035) seasons when compared to the post-melt season (Table S5). δ^{13}C-POC ranged from -
360 38.8 to -20.8‰ (Fig. 4b), and increased with distance downstream (χ^2_1=6.23; p=0.013), but with a significant interaction between distance and season (χ^2_3=10.70; p=0.013; Table S4). Δ^{14}C-DOC became more enriched with increasing distance downstream (χ^2_1=6.03; p=0.014) but with high variability at the headwater site, particularly during the melt season (-554‰ to +7‰; n = 8) (Figs. 3b and 4a and 5a). Δ^{14}C-DOC also varied (χ^2_3=23.70; p=0<001), with values most depleted during winter compared to other seasons (p=0.020 to 0.001 for various comparisons) (Fig. 5a3b, Tables S4, S5). In addition, Δ^{14}C-DOC
365 showed a modest negative association with protein-like DOM (linear model R$^2_{adj}$ = 0.17, F$_{1,39}$ = 8.212, p = 0.007) (Fig. 5b3c). Similar to Δ^{14}C-DOC, Δ^{14}C-POC exhibited a large range in values, from -550‰ to -108‰ (Fig. 4b). However, in contrast to Δ^{14}C-DOC the large variation in Δ^{14}C-POC values was not associated with significant seasonal or spatial differences between samples (Fig. 4, Table S4).

3.1.3 An integrative assessment of DOM composition across sites

370 A principal component analysis (PCA) exploring DOM composition across sites identified eight principal components with 64% of the observed variation being explained by the first two principal component axes (Fig. 65). Principal component 1 (PC1) explained 49% of sample variance, with humic-like PARAFAC components, DOC concentration and HIX (humification) loading positively on this axis, and protein-like PARAFAC components, BIX (biological origin), FI (microbial origin), and S$_{275-295}$ (declining molecular weight) loading negatively. Sites generally plotted along PC1 according to their
375 distance from glacier termini, with headwater and near sites more frequently having negative PC1 scores, and far sites having

12

more positive PC1 scores (Fig. ~~6~~5). PC2 explained 14% of sample variance and was positively associated with δ^{13}C-DOC and negatively associated with SUVA$_{254}$ (aromaticity). A passive overlay of deuterium excess was negatively associated with PC1, and positively associated with PC2 (Fig. ~~6~~5).

3.2 Microbial assemblage characterization and its controls over space and time

380 ~~Of our target sample set, we successfully obtained sequences from 72 samples, with ASV richness ranging from 81 to 9,634, and read counts ranging from 5,066 to 409,740; inspection of Rarefaction curves confirms that a plateau were reached for all included samples (i.e., those with greater than 5,000 reads; Fig. S3).~~ Generally, microbial assemblages shared similar dominant phyla and orders across sites and seasons with the top ten most abundant phyla across all samples being: Acidobacteriota, Actinobacteriota, Bacteroidota, Bdellovibrionota, Chloroflexi, Cyanobacteria, Firmicutes, Plantomycetota, Proteobacteria, and

385 Verrucomicrobiota (Fig. S4). At near and far sites in the Sunwapta-Athabasca and North Saskatchewan rivers, these ten phyla collectively described between 80–88% of the resolved microbial assemblage composition (Fig. S4). Major microbial orders were dominated by Burkholderiales, Chitinophagales, Cytophagales, Flavobacteriales, Frankiales, Microtrichales, Sphingobacteriales, Synechococcales and Vicinamibacterales) (Fig. S5), with microorganisms related to Burkholderiales appearing most dominant, particularly in August at sites closer to the headwaters. Cumulatively, the top 10 orders accounted

390 for 56 % of the total microbial assemblage composition. To explore taxonomic variation at a finer scale, we investigated shared ASVs across distance ranges (Fig ~~7a~~6a). This assessment revealed a core microbial assemblage, shared among all our samples, comprised of 1409 ASVs total, with the top 10 most abundant ASVs belonging to families Comamonadaceae, Cyanobiaceae, Gallionellaceae, Ilumatobacteraceae, Sporichthyaceae, Alcaligenaceae, Methylophilaceae and Flavobacteriaceae. While this core assemblage only represented 3.4% of all identified ASVs (Fig. ~~7a~~6a), it made up a large fraction of relative abundance at

395 each site (between 25–80%; Fig. ~~7b~~6b), with a general decreased prevalence of the core assemblage at the far sites, when compared to headwaters and near. Accordingly, microbial assemblage diversity was highest at the far sites during all seasons (Fig. S5). Indeed, near sites showed a reduction in diversity from a median of 5.7 at premelt to a median of 4.3 post-melt, whereas far sites increased in diversity throughout the melt season from a median pre-melt diversity value of 6.5 to 6.8 at post melt. Further, ~~and~~ a comparison of microbial diversity between samples (beta diversity) showed that assemblage composition

400 shifted with movement from headwater and near to far sites (R^2 = 0.09, p < 0.001) (Fig. ~~8~~7, Table S7). ~~Communities~~ Assemblages were also distinct across rivers (R^2 = 0.08, p < 0.001; comparing the Athabasca, Sunwapta, and North Saskatchewan) and different sampling years (R^2 = 0.06, p < 0.001; comparing 2019, 2020, 2021) with each river and year being significantly different from one other (p<0.01) (Fig. S7, Table S7).

405 We used a distance-based RDA to assess how microbial assemblages varied across environmental gradients, to better understand the role of environment in structuring assemblages at each of our sites. Removal of environmental variables with VIF>10 reduced the initially-considered factors described in the Methods (n=32) to: % protein-like DOM, water temperature,

13

DOC concentration, POC concentration, δ^{13}C-DOC, δ^{18}O-H$_2$O, deuterium excess, S$_{275\text{-}295}$, SUVA$_{254}$, TN, TP, and specific conductance (n=12). Following backward selection, the final RDA described 9.1% (adjusted; see Methods) of microbial
410 assemblage structure, with % protein-like DOM, water temperature, specific conductance, POC and deuterium excess identified as significant predictor variables ($p < 0.001$) (Fig. ~~9~~8). RDA axis 1 (RDA1) described a gradient of apparent high elevation (e.g., glacial ice, snow) water source inputs, with deuterium excess and protein-like DOM negatively correlated, and specific conductance and water temperature positively correlated with this axis (Fig. ~~9~~8). RDA axis 2 (RDA2) showed water temperature loading negatively on this axis and POC loading positively (Fig. ~~9~~8). Headwater sites plotted negatively on RDA1
415 and positively on RDA2, whereas far sites tended to plot positively on RDA1. Overall, headwater microbial ~~communities~~ assemblages were associated with relatively higher proportions of protein-like DOM, deuterium excess, and POC but lower specific conductance and water temperature compared to ~~communities~~ assemblages at the far sites (Fig. ~~9~~8).

3.2.1 Indicator species analysis

An ISA resolved three strong (indicator value (IV) > 0.8, $p < 0.05$) indicator species for headwater sites and two strong indicator
420 species for far sites. There were no strong indicator species for near sites at this IV threshold. Indicator species for the headwater sites were identified as a species from the genus *Cryobacterium* (IV = 0.89), a~~n~~ ASV ~~species~~ from family Beggiatoaceae (IV = 0.82), and a~~n~~ ASV ~~species~~ from family Microbacteriaceae (IV = 0.87). Far indicators were a species from family Sporichthyaceae (IV = 0.83), and a species in the genus *Cyanobium_PCC-6307* (IV = 0.83). Correlations between ASV abundance and deuterium excess revealed that taxa indicative of headwater environments were strongly positively correlated
425 with deuterium excess (positive ρ values), while taxa indicative of far environments showed a negative correlation (negative ρ values; Fig. ~~10~~9).

4 Discussion

4.1 Changing OM quantity and character driven by increased soil development downstream

Stream OM originates from two primary sources: 1) *in situ* primary production of OM from autotrophic microbes or
430 macrophytes (autochthonous carbon); or 2) OM transported into the stream system from outside sources (allochthonous carbon) such as nearby vegetation and soils (Hinton et al., 1997, 1998; Tanentzap et al., 2014; Table S8). In glacially-fed streams, glacially sourced OM also contributes to the allochthonous carbon pool (Hood et al., 2015a). However, glaciers are associated with a series of variable OM sources, as a result of *in situ* microbial metabolism on the glacier surface (supraglacial) and at the glacier bed (subglacial) (Hotaling et al., 2017; Stibal et al., 2012), as well as from windblown deposition on the
435 snow and ice surface and comminuted sediments and bedrock at the glacier bed (Hood et al., 2020; Stubbins et al., 2012). Thus, the changing water source contributions to streams is a critical determinant of fluvial OM composition, both in alpine environments and elsewhere (Fasching et al., 2016).

14

This study identified a shift in OC quantity and OM character with increasing distance downstream from glaciers and thus
440   declining relative contributions of glacial meltwater and associated OM to streamflow. Low DOC concentrations in our
mountain headwater streams, which drain catchments lacking developed soils and where dilute glacial meltwaters are the
primary source of allochthonous carbon, are in agreement with previous work from the Alps (Singer et al., 2012), Tibetan
Plateau (Zhang et al., 2018; Zhou et al., 2019), Canadian Rockies (Lafrenière et al., 2004), and the Greenland Ice sheet
(Kellerman et al., 2020). In contrast, the large relative contribution of POC to the headwater TOC pool is consistent with
445   increased erosional processes in high slope glacial margin environments, export of glacially derived sediments (Hood et al.,
2020), and higher rates of particle re-suspension in these high gradient, turbulent, reaches (Marcus et al., 1992). At the
headwaters, the protein-like character of the DOM pool suggests dominant contributions from microbial production or
reworking of DOM, either on the glacier surface or at the bed, as has been found in many other glacierized regions (Zhou et
al., 2019; Dubnick et al., 2010; Hood et al., 2009; Stubbins et al., 2012; Pain et al., 2020; Singer et al., 2012). Increasing DOC
450   concentrations and a shift from protein-like to humic-like DOM with increasing distance downstream supports increasing
contributions of allochthonous carbon from surrounding vegetation and more developed soils (see also, Zhou et al., 2019). The
conclusion that headwater sites receive a majority of their OM directly from the glacier, and downstream locations gain
additional OM contributions derived from catchment soils, is supported by declines in deuterium excess with movement
downstream (Fig. ~~S1~~S2, Table S4), and thus an inferred switch to increasing water contributions of rainfall and lower-elevation
455   sourced precipitation (Bershaw and Lechler, 2019; Bershaw et al., 2020).

4.2 Stream POC sourced from plant carbon with potential additions from glacier microbes

Compared to the DOC pool, the POC pool displayed less isotopic variation, pointing to a more consistent POC source to
streams. Across seasons and with increasing distance downstream, the POC pool was consistently aged (Δ^{14}C-POC = -550‰
to -108‰). At the headwaters, this depletion likely indicates sourcing from glacial export of overridden vegetation (Bhatia et
460   al., 2013), or fossil fuel products (Stubbins et al., 2012) and the heterotopic consumption of fossil fuels by cryoconite microbes
(Margesin et al., 2002). Further downstream, radiocarbon depleted POC could be sourced from the addition of water from
aged soil margins, or glacially exported aged POM that has persisted through the stream network (Hood et al., 2020). However,
save for the headwater site during the pre-melt period, δ^{13}C-POC indicated POM primarily of terrestrial origin (δ^{13}C‰ = -26
to -28‰), with occasional slight depletions at headwater and near sites (δ^{13}C‰ = -29 to -30‰) pointing to possible contribution
465   from subglacial chemosynthetic biofilms (Table S8). Indeed, if some of the aged POM is sourced from subglacial microbes,
this fraction of POM may be more accessible to recipient food webs than aged terrestrial POM (Brett et al., 2017), though
relative contributions through our transects is likely small. The pre-melt headwater sample was uniquely δ^{13}C-enriched
compared to other POM samples, which may suggest microbial re-working of depleted ~~C~~ carbon sources as a more dominant
POM source at this time.

15

4.3 Seasonal patterns in DOM from headwaters to downstream reaches

Glacial headwaters

Over the past two decades, studies from polar and alpine regions across the globe have led to the characterization of glacial DOM as universally dilute, of microbial origin, and old (i.e. radiocarbon depleted) (Bhatia et al., 2013; Hood et al., 2009). Similarly, we found that DOM was consistently most protein-like in headwater reaches (Table S4), but with compositional variation during the melt season (Fig. 2). Our results contrast somewhat with other studies where melt-season shifts in glacial stream DOM character from relatively more humic-like to more protein-like have been associated with efficient subglacial channels during the peak melt season (Kellerman et al., 2020). For example, DOM fluorescence in the outflow draining Leverett Glacier, a large land-terminating glacier of the Greenland Ice Sheet, was relatively more humic-like in the early season, when waters draining subglacial flow paths access terrestrial material from previously overridden soils and bedrock dominated stream contributions (Kellerman et al., 2020). In comparison, during peak melt flow, when supraglacial inputs dominated, Leverett Glacier outflow DOM had a distinctly more protein-like fluorescence signature (Kellerman et al., 2020). Similarly, protein-like fluorescence increased from the pre-melt to the melt period in waters draining the Mendenhall Glacier, Alaska (Spencer et al. 2014). At these Rocky Mountain glacier sites, the variability in DOM source during the melt season may point to temporally patchy interactions with the overridden vegetation and paleosols known to be prevalent in this region (Luckman et al. 2020).

During the pre-melt period, water at the Athabasca glacier terminus is predominately sourced from the distributed subglacial drainage network (Arendt, 2015), with DOC that was aged (Δ^{14}C-DOC = -175‰), with δ^{13}C-DOC of -25.5‰ (Fig. 4). These carbon isotopic signatures, in conjunction with the consistent protein-like DOM fluorescence, suggest microbial reworking of previously overridden vegetation and soils at the glacier bed (Bhatia et al., 2013; Dubnick et al., 2010; see also Table S8). During the melt season, headwater δ^{13}C-DOC shows substantial variation, in line with the DOM compositional variation described above. Four of six Δ^{14}C-DOC samples from this period were relatively aged (Fig. 4); together with the relatively protein-like composition of the DOM pool, this isotopic variation is consistent with a range of sources including: a) chemolithoautotrophy tied to microbial heterotrophic consumption of ancient vegetation and soil at the glacier bed (Hood et al., 2009); b) microbial re-working of over-ridden vegetation; or c) microbial incorporation of radiocarbon-dead fossil fuel combustion products deposited on the glacier surface (McCrimmon et al., 2018). Previous work in alpine glacial systems in both Alaska (Stubbins et al., 2012) and Tibet (Spencer et al., 2014) have found the latter to substantially contribute to supraglacial DOC pools during peak melt periods. In a subset of melt season samples, however, headwater Δ^{14}C-DOC was enriched (Fig. 4). This could be indicative of recent contributions from ~~recent photosynthetic~~ supraglacial photosynthetic ~~microbial~~ microbes~~communities~~ (Kellerman et al., 2021; Smith et al., 2017; Stibal et al., 2012) or contributions from wildfire-derived soot present on the glacier surface (Aubry-Wake et al., 2022; Nizam et al., 2020). Overall, the range of

DOM composition, δ^{13}C-DOC, and Δ^{14}C-DOC points to striking heterogeneity of water sources draining to the glacial outflow at this site.

505 *Transit downstream*

With transit downstream, DOM becomes overall more humic like (Table S4), but with seasonal variability in character. During the pre-melt period, inputs of enriched Δ^{14}C-DOC were coupled with δ^{13}C-DOC values consistent with terrestrial OM inputs (-25‰ to -27‰) at the near and mid sites, likely indicative of snowpack melt draining surficial soils, leading to pulses of concentrated modern, terrestrial-origin DOM delivery to streams (Fig. 4). This flushing of concentrated DOM from soils was

510 the likely cause of the spike in DOC concentration observed during the pre-melt season at downstream sites in 2019 (Fig. 2), when sampling captured the spring freshet. This process has been observed previously at Bow River from 1998–2000, when the highest DOC concentrations were found to occur during the initial snowpack melt and, as in this study, were followed by a decline in river DOC concentrations (Lafrenière and Sharp, 2004). These isotopic signatures were also tied to higher proportional inputs of humic-like DOM (Fig. 4).

515

During the melt season, a proportional increase in protein-like fluorescence at the near, mid, and far sites was coupled with DOM pools at near and mid sites switching from being consistent with allochthonous terrestrial inputs (δ^{13}C-DOC = -25 ‰ to -29 ‰) to showing a clear autochthonous signature reflective of chemo- or photosynthetic OM production (δ^{13}C-DOC ranging from -35‰ to -20‰; Figs. 3 and 4). Near and mid sites were also characterized by DOM that was often Δ^{14}C-DOC depleted.

520 This trend may reflect increasing *in situ* production by microbial photoautotrophs, as evidenced by the presence of cyanobacteria DNA in the microbial amplicon libraries from these sites (Fig. S3S4), or microbial re-working of humic-like DOM, either within the stream or in catchment soils (Fig. 4). Aged carbon downstream likely represents the mixing of either: a) ancient glacially exported material from the headwaters persisting downstream or b) additions from deeper, older soils (Shi et al., 2020). During the post-melt period, stream water at the near and mid distances was either aged (Δ^{14}C-DOC = -630‰, -

525 400‰) with a δ^{13}C-DOC terrestrial signature (-28‰, -29‰), consistent with OM contributions from deeper soils when discharge is declining, or slightly more modern (Δ^{14}C-DOC = -193‰, -110‰) and δ^{13}C-enriched (-22‰), consistent with incorporation of autochthonous primary production into the DOM pool (Fig. 4). Future studies could consider a mixing model to add more specificity to these assessments, via the inclusion of additional tracers to resolve the multiple endmembers of this system.

530 **4.4 Implications of inferred composition for OM lability**

The transition from recently produced, low molecular weight, protein-like DOM to high molecular weight, humic-like DOM with movement downstream has implications for DOM lability. Protein-like DOM is associated with free amino acids and proteinaceous compounds which are generally considered to be more available for heterotrophic microbial consumption

Formatted: Font: Italic

(Coble, 1996), while factors such as decreasing molecular weight ($S_{275-295}$) (Fig. 6̶5, Table S3) are also associated with increasing OM lability (Moran and Zepp, 1997; Patriarca et al., 2021). In previous studies of glacial DOM, paired high resolution mass spectrometry and UV-Vis spectrometry have shown that protein-like fluorescence is associated with unsaturated aliphatic compounds, identified as being peptide- and lipid-like (Kellerman et al., 2020, 2021; Stubbins et al., 2012; Zhou et al., 2019), which have been found to be a common contributor to glacier DOM pools in many regions (Singer et al., 2012; Bhatia et al., 2013; Kellerman et al., 2021; Stubbins et al., 2012; Zhou et al., 2019). In contrast, humic-like DOM is associated with complex material (e.g., increased lignin content; Mann et al., 2016; Zhou et al., 2019) and thus is generally considered to be a more recalcitrant fraction of DOM. This shift in lability has important implications for stream ecosystems, because microbial consumption of DOM can provide an energetic transfer to higher trophic levels (e.g., Fellman et al., 2015), with labile DOM being linked to increased microbial productivity (Pontiller et al., 2020). Labile OM released at the headwater site could also initiate priming of the OM pool, resulting in increased microbial consumption of recalcitrant soil-derived OM (Bingeman et al., 1953; Guenet et al., 2010). Notably, the importance of priming has yet to be assessed in glacially fed streams (Bengtsson et al., 2018). However, despite the shift in apparent bulk DOM lability with movement downstream, one additional consideration is the low overall DOC concentration at headwater sites. Although downstream sites had lower proportions of protein-like DOM, these sites had higher DOC concentrations overall. A rough calculation to compare between sites yields an estimated mean 0.28 mg L^{-1} of protein-like DOM at downstream sites, compared to ~0.21 mg L^{-1} at the headwaters (using the mean DOC and % protein-like DOM for each distance bin). Therefore, although DOM may have been more accessible to microbes on a proportional basis in the headwaters, overall OM processing may still have been higher downstream.

4.5 Controls on microbial assemblage structure with transit downstream

Microbial ~~communities~~ assemblages and OM pools are inherently linked since microbes contribute both to the creation of OM and its consumption (Kujawinski, 2011). To explore possible coupling between microbial assemblages and stream OM, we investigated how assemblages shifted with increasing distance from glaciers and coupled changes in OM source, OM character, and other physicochemical characteristics. Across all sites and seasons, 10 phyla were found to account for 80–88% of assemblage composition (Fig. S̶3̶S4). While some of these phyla (Actinobacteria, Acidobacteriota, Cyanobacteria, Bacteroidota, and Proteobacteria) are ubiquitous in freshwater (Tamames et al., 2010), many (Proteobacteria, Bacteroidota, Acidobacteriota, Actinobacteriota, Chloroflexi, Cyanobacteria and Firmicutes, Plantomycetota) are also commonly identified as being dominant in glacial ecosystems and in glacially-fed streams (Boetius et al., 2015; Bourquin et al., 2022; Hotaling et al., 2019). These glacially associated phyla are known to include taxa that are adapted to the environmental conditions typical of glacial environments, such as oligotrophy and cold temperatures (Bourquin et al., 2022). At a finer taxonomic resolution, the orders Cytophagales, Chitinophagales, Vicinamibacterales, Burkholderiales, and Flavobacteriales are also commonly found in glacially fed waters (Kohler et al., 2020, Brandani et al., 2023, Guo et al., 2024). Burlholderiales and Flavobacteriales are known for their contributions to organic matter cycling in oligotrophic systems such as these (Guo et al., 2024).

18

Interestingly, the order Sphingomonadales has also been shown to be significantly correlated with suspended sediment concentrations released from the Greenland Ice Sheet (Dubnick et al., 2017). Although our system is situated within the Canadian Rocky Mountains, similar controls on the incorporation of sediment occur as glaciers melt, seeding downstream rivers with sediment-associated microorganisms.

570

Poor evidence for species sorting along glacier to downstream gradients

At the ASV level, we see some evidence for structured changes in microbial assemblages along the connected headwater to downstream reaches that we investigated. First, within site (alpha) and between site (beta) diversity increased with increasing distance from the glacier (Figs. 76, Fig. S6). This result is consistent with a previous study in the Alps, where lower alpha

575 diversity near glaciers was attributed to a decrease in the diversity of microbial source pools at higher elevations (e.g., lower groundwater contributions) and/or harsher upstream environmental conditions (Wilhelm et al., 2013). Second, we identified specific microbial indicator species for specific to each of the headwater and downstream sites. Headwater indicators Microbacteriaceae *sp.* and Microbacteriaceae *Cryobacterium sp.* are heterotrophs that are commonly found within glacial cryoconite holes and are believed to possess specific adaptations for cold temperatures and nutrient-poor conditions (Liu et al.,

580 2020). The third headwater microbial indicator was a sulphur oxidizing chemolithotroph (Beggiatoaceae *sp.*), likely sourced from the subglacial environment where chemosynthesis is common (Anesio et al., 2017). The identification of these indicator species suggests that unique microbes (sourced from both the supraglacial and subglacial environment) may be seeding the fluvial microbial assemblage at the glacial headwaters (Wilhelm et al. 2013; Bhatia et al., 2006). Third, redundancy analysis identified a series of physicochemical variables – including protein-like DOM, water temperature, POC concentration, specific

585 conductance, and deuterium excess – that were significantly associated with microbial assemblage composition across sites (Fig. 98). Of these environmental controls, DOM character can select for different specialized heterotrophic microbes (Judd et al., 2006), water temperature broadly controls rates of microbial activity (D'Amico et al., 2006), and POC can shape bacterial extracellular enzyme requirements and thus, microbial assemblage composition (Kellogg and Deming, 2014). From these lines of evidence, we conclude that glaciers are providing a biotic source of novel microbes to glacially-fed streams in the Rocky

590 Mountains (see also Wilhelm et al., 2013; Bhatia et al., 2006), but that the association between assemblages structure and environment is modest, with the RDA explained only a small amount (9%) of the observed variation in microbial assemblages across sites (Fig. 98).

Dispersal and increasing cell sources with transit downstream

595 In addition to the overall modest RDA results, perMANOVA tests of species divergence among site bins (i.e., beta diversity) indicated that spatial variation only explained a small proportion of assemblage composition, suggesting a high degree of similarity between microbial communitiesassemblages ($R^2 = 0.09$, $p < 0.001$, Table S7). This low overall explanatory power of specific environmental controls, combined with a lack of strong assemblage divergence between environmentally disparate

19

sites, is consistent with a recent synthesis effort that concluded environmental drivers are not always good predictors for
600   microbial assemblage composition in streams (Zeglin, 2015).

This lack of strong control from among our suite of environmental variables is also consistent with patterns observed for the
"core" group of microbial ASVs that was ubiquitous across all distance ranges (headwater, near, far) examined in this study.
While this core ASV group accounted for only ~3% of the total identified ASVs, it represented a large proportion of average
605   relative ASV abundance across sites, ranging from a median of 70% of the total assemblage relative abundance at headwater
locations to 55% at downstream sites (Fig. 87). Across all sites, the most abundant (top 10) core ASVs, identified to the lowest
taxonomic level available, display diverse metabolisms, with some heterotopic taxa that are considered to be generalists (e.g.,
Flavobacterium sp. (Zheng et al., 2019)*, Sporichthyaceae*), specialists for methanol consumption (Methylophilaceae (Beck et
al., 2014)), specialists for consumption of terrestrial carbon (*Alcaligenaceae sp.*) and autotrophic taxa, including both
610   photoautotrophs (e.g., cyanobacteria) and chemoautotrophs (e.g., iron oxidizing Gallionellaceae (Hallbeck and Pedersen,
2014)). Increases in alpha diversity and declining relative importance of the "core" assemblage from headwaters to downstream
sites indicates more diverse communities assemblages downstream, consistent with an increased variety of microbial sources
of microbial communities from the surrounding terrestrial environment (Figs. 76, S6). However, the strong persistence of the
core assemblage across our transects also reinforces that rivers are highly connected environments that can facilitate high rates
615   of dispersal (Tonkin et al., 2018), albeit in a unidirectional fashion. As such, mass effects can be strong drivers of microbial
assemblage composition in fluvial networks resulting in assemblage homogenization and, overall, decreased species sorting
(Crump et al., 2007; Evans et al., 2017; Leibold et al., 2004; Pandit et al., 2009). These findings contrast with those from
studies of more isolated environments such as lakes (Logue et al., 2010; Van der Gucht et al., 2008) and soils (Fierer et al.,
2006), where longer residence times better enables environmental divergence between sites to drive divergence in microbial
620   assemblage composition. In our glacially-fed systems, particularly, we find that while local environmental conditions show
some association with microbial assemblage composition, mass effects (homogenization by high rates of dispersal) are likely
more influential, suggesting a clear ecological connection from glacial outflows to 100-km downstream sites, despite striking
environmental change.

5 Conclusions

625   This study illustrates that fluvial OM quantity and quality changes along stream transects from glacier headwaters to ~100 km
downstream in the Rocky Mountains. These changes occur as a result of shifting inputs from different OM sources, with
headwater sites adjacent to the glacier containing DOM that is compositionally consistent with predominantly autotrophic
inputs (chemosynthesis and photosynthesis) and microbial reworking of terrestrially sourced OM that is aged and likely labile.
Comparatively, the downstream DOM pool was predominately humic-like, but exhibited seasonal shifts in apparent OM source
630   with some allochthonous inputs in the pre-glacial melt and post-glacial melt seasons, and autochthonous sources increasing at

the height of the melt season. This study also identified that a portion of glacially exported POC may be sourced from microbial activity, and thus is potentially accessible to downstream food webs. In contrast to these clear environmental gradients, we found that, despite evidence for glacial seeding of headwater microbial ~~communities~~assemblages, mass effects appeared to enable dispersal of a persistent core microbial group throughout our stream transects from the glacial headwaters to ~100 km
635 downstream. Increasing microbial assemblage diversity with movement downstream, in the absence of a strong correlation with in-stream physical and chemical condition, points to a greater diversity of cell sources (i.e., increasing lateral inputs) along our study continuum.

Overall, findings from this work will enable better predictions about the impacts of glacial retreat on stream ecosystems, and
640 the loss of labile OM inputs in alpine headwater regions. In the future, with increased glacier retreat in the Canadian Rockies, glacially-fed rivers will shift from a glacier ice melt regime towards one dominated by seasonal snow and rainwater inputs (Pradhananga and Pomeroy, 2022). Necessarily, these changes will be accompanied by increases in surrounding soil development and vegetation cover. The likely result is a higher proportion of humic-like DOM at headwater sites, a potential loss of glacially-derived POM bioavailable to downstream primary consumer organisms (Cotner and Biddanda, 2002), and
645 changes in other environmental parameters (temperature, chemistry) identified in this study as being important correlates for stream microbial assemblages. At the same time, a loss of glacially exported microbes will alter the seed pool at headwater sites, which appears to persist far downstream, thus potentially altering the core assemblage that is characteristic of this glacially-fed river system. Overall, glacier retreat and eventual deglaciation appears poised to cause a loss of glacial seeding of microbial assemblages in headwaters of the Canadian Rockies, similar to predictions for other glacierized Alpine regions
650 (Hotaling et al., 2017). This loss of a unique source pool to the base of stream food webs could have a negative impact on overall biodiversity and ecosystem function, particularly if this loss of inputs decreases the functional breadth of these systems.

Data availability

All water chemistry and organic matter datasets generated and analysed in this study are available on PANGAEA repository
655 (Felden et al., 2023)(PDI-35664 and Serbu et al., 2024). Microbial 16S rRNA gene sequences generated and used in this study can be accessed from the NCBI database, using accession number PRJNA995204.

Author contributions

VLStL, JAS, SET, and MPB designed the field program, and SET and MPB designed this study. HFD and JAS led the field
660 sampling campaigns, and HFD, MAC, and JAS conducted the laboratory analysis. MAC built the 16S rRNA gene libraries and conducted the bioinformatic analyses. HFD conducted all other data and statistical analyses, and visualized the results. HFD wrote the paper with input from SET and MPB, and all authors provided comments on the manuscript.

Competing interests

665   The authors declare that they have no conflict of interest.

References

Anderson, S. and Radić, V.: Identification of local water resource vulnerability to rapid deglaciation in Alberta, Nat. Clim.
685 Chang., 10, 933–938, https://doi.org/10.1038/s41558-020-0863-4, 2020.

Anesio, A. M., Lutz, S., Chrismas, N. A. M., and Benning, L. G.: The microbiome of glaciers and ice sheets, npj Biofilms
Microbiomes, 3, 1–11, https://doi.org/10.1038/s41522-017-0019-0, 2017.

Water Level and Flow - Environment Canada: https://wateroffice.ec.gc.ca/index_e.html, last access: 8 August 2022.

Arendt, C. A.: The Hydrologic Evolution of Glacial Meltwater: Insights and Implications from Alpine and Arctic Glaciers,
690 190, n.d.

Arendt, C. A., Stevenson, E. I., and Aciego, S. M.: Hydrologic controls on radiogenic Sr in meltwater from an alpine glacier
system: Athabasca Glacier, Canada, Applied Geochemistry, 69, 42–49, https://doi.org/10.1016/j.apgeochem.2016.04.002,
2016.

Aubry-Wake, C., Bertoncini, A., and Pomeroy, J. W.: Fire and Ice: The Impact of Wildfire-Affected Albedo and Irradiance
695 on Glacier Melt, Earth's Future, 10, e2022EF002685, https://doi.org/10.1029/2022EF002685, 2022.

Bates, D., Mächler, M., Bolker, B., and Walker, S.: Fitting Linear Mixed-Effects Models Using lme4, Journal of Statistical
Software, 67, 1 - 48, 10.18637/jss.v067.i01, 2015.

Beck, D. A. C., McTaggart, T. L., Setboonsarng, U., Vorobev, A., Kalyuzhnaya, M. G., Ivanova, N., Goodwin, L., Woyke, T.,
Lidstrom, M. E., and Chistoserdova, L.: The Expanded Diversity of Methylophilaceae from Lake Washington through
700 Cultivation and Genomic Sequencing of Novel Ecotypes, PLOS ONE, 9, e102458,
https://doi.org/10.1371/journal.pone.0102458, 2014.

Bengtsson, M. M., Attermeyer, K., and Catalán, N.: Interactive effects on organic matter processing from soils to the ocean:
are priming effects relevant in aquatic ecosystems?, Hydrobiologia, 822, 1–17, https://doi.org/10.1007/s10750-018-3672-2,
2018.

705 Bernhardt, E. S., Savoy, P., Vlah, M. J., Appling, A. P., Koenig, L. E., Hall, R. O., Arroita, M., Blaszczak, J. R., Carter, A.
M., Cohen, M., Harvey, J. W., Heffernan, J. B., Helton, A. M., Hosen, J. D., Kirk, L., McDowell, W. H., Stanley, E. H.,
Yackulic, C. B., and Grimm, N. B.: Light and flow regimes regulate the metabolism of rivers, Proceedings of the National
Academy of Sciences, 119, e2121976119, https://doi.org/10.1073/pnas.2121976119, 2022.

Bershaw, J. and Lechler, A. R.: The isotopic composition of meteoric water along altitudinal transects in the Tian Shan of
710 Central Asia, Chemical Geology, 516, 68–78, 2019.

Bershaw, J., Hansen, D. D., and Schauer, A. J.: Deuterium excess and 17O-excess variability in meteoric water across the
Pacific Northwest, USA, Tellus B: Chemical and Physical Meteorology, 72, 1–17,
https://doi.org/10.1080/16000889.2020.1773722, 2020.

Bhatia, M. P., Das, S. B., Longnecker, K., Charette, M. A., and Kujawinski, E. B.: Molecular characterization of dissolved
715 organic matter associated with the Greenland ice sheet, Geochimica et Cosmochimica Acta, 74, 3768–3784,
https://doi.org/10.1016/j.gca.2010.03.035, 2010.

Bhatia, M. P., Das, S. B., Xu, L., Charette, M. A., Wadham, J. L., and Kujawinski, E. B.: Organic carbon export from the
Greenland ice sheet, Geochimica et Cosmochimica Acta, 109, 329–344, https://doi.org/10.1016/j.gca.2013.02.006, 2013.

23

Bingeman, C. W., Varner, J. E., and Martin, W. P.: The Effect of the Addition of Organic Materials on the Decomposition of an Organic Soil, Soil Science Society of America Journal, 17, 34–38, https://doi.org/10.2136/sssaj1953.03615995001700010008x, 1953.

Boetius, A., Anesio, A. M., Deming, J. W., Mikucki, J. A., and Rapp, J. Z.: Microbial ecology of the cryosphere: sea ice and glacial habitats, Nat Rev Microbiol, 13, 677–690, https://doi.org/10.1038/nrmicro3522, 2015.

Bolch, T., Menounos, B., and Wheate, R.: Landsat-based inventory of glaciers in western Canada, 1985–2005, Remote Sensing of Environment, 114, 127–137, https://doi.org/10.1016/j.rse.2009.08.015, 2010.

Boral, S., Sen, I. S., Ghosal, D., Peucker-Ehrenbrink, B., and Hemingway, J. D.: Stable water isotope modeling reveals spatio-temporal variability of glacier meltwater contributions to Ganges River headwaters, Journal of Hydrology, 577, 123983, https://doi.org/10.1016/j.jhydrol.2019.123983, 2019.

Bourquin, M., Busi, S. B., Fodelianakis, S., Peter, H., Washburne, A., Kohler, T. J., Ezzat, L., Michoud, G., Wilmes, P., and Battin, T. J.: The microbiome of cryospheric ecosystems, Nat Commun, 13, 3087, https://doi.org/10.1038/s41467-022-30816-4, 2022.

Brandani, J., Peter, H., Fodelianakis, S., Kohler, T. J., Bourquin, M., Michoud, G., Busi, S. B., Ezzat, L., Lane, S., and Battin, T. J.: Homogeneous Environmental Selection Structures the Bacterial Communities of Benthic Biofilms in Proglacial Floodplain Streams, Appl Environ Microbiol, 89, e0201022, 10.1128/aem.02010-22, 2023.

Cáceres, M. D. and Legendre, P.: Associations between species and groups of sites: indices and statistical inference, Ecology, 90, 3566–3574, https://doi.org/10.1890/08-1823.1, 2009.

Campbell, D. H., Clow, D. W., Ingersoll, G. P., Mast, M. A., Spahr, N. E., and Turk, J. T.: Processes Controlling the Chemistry of Two Snowmelt-Dominated Streams in the Rocky Mountains, Water Resources Research, 31, 2811–2821, https://doi.org/10.1029/95WR02037, 1995.

Clarke, G. K. C., Jarosch, A. H., Anslow, F. S., Radić, V., and Menounos, B.: Projected deglaciation of western Canada in the twenty-first century, Nature Geosci, 8, 372–377, https://doi.org/10.1038/ngeo2407, 2015.

Coble, P. G.: Characterization of marine and terrestrial DOM in seawater using excitation-emission matrix spectroscopy, Marine Chemistry, 51, 325–346, https://doi.org/10.1016/0304-4203(95)00062-3, 1996.

Crump, B. C., Adams, H. E., Hobbie, J. E., and Kling, G. W.: Biogeography of Bacterioplankton in Lakes and Streams of an Arctic Tundra Catchment, Ecology, 88, 1365–1378, https://doi.org/10.1890/06-0387, 2007.

Cui, X., Bianchi, T. S., Jaeger, J. M., and Smith, R. W.: Biospheric and petrogenic organic carbon flux along southeast Alaska, Earth Planet. Sc. Lett., 452, 238-246, https://doi.org/10.1016/j.epsl.2016.08.002, 2016.

D'Amico, S., Collins, T., Marx, J.-C., Feller, G., and Gerday, C.: Psychrophilic microorganisms: challenges for life, EMBO Rep, 7, 385–389, https://doi.org/10.1038/sj.embor.7400662, 2006.

D'Andrilli, J., Cooper, W. T., Foreman, C. M., and Marshall, A. G.: An ultrahigh-resolution mass spectrometry index to estimate natural organic matter lability, Rapid Communications in Mass Spectrometry, 29, 2385–2401, https://doi.org/10.1002/rcm.7400, 2015.

Davis, N. M., Proctor, D. M., Holmes, S. P., Relman, D. A., and Callahan, B. J.: Simple statistical identification and removal of contaminant sequences in marker-gene and metagenomics data, https://doi.org/10.1101/221499, 25 July 2018.

24

755 Dubnick, A., Barker, J., Sharp, M., Wadham, J., Grzegorz, L., Telling, J., Fitzsimons, S., and Jackson, M.: Characterization of dissolved organic matter (DOM) from glacial environments using total fluorescence spectroscopy and parallel factor analysis, Annals of Glaciology, 51, 111–122, https://doi.org/10.3189/172756411795931912, 2010a.

Dubnick, A., Barker, J., Sharp, M., Wadham, J., Lis, G., Telling, J., Fitzsimons, S., and Jackson, M.: Characterization of dissolved organic matter (DOM) from glacial environments using total fluorescence spectroscopy and parallel factor analysis,
760 Annals of Glaciology, 51, 111–122, https://doi.org/10.3189/172756411795931912, 2010b.

Dubnick, A., Kazemi, S., Sharp, M., Wadham, J., Hawkings, J., Beaton, A., and Lanoil, B.: Hydrological controls on glacially exported microbial assemblages, Journal of Geophysical Research: Biogeosciences, 122, 1049-1061, https://doi.org/10.1002/2016JG003685, 2017.

Dufrêne, M. and Legendre, P.: Species Assemblages and Indicator Species:the Need for a Flexible Asymmetrical Approach,
765 Ecological Monographs, 67, 345–366, https://doi.org/10.1890/0012-9615(1997)067[0345:SAAIST]2.0.CO;2, 1997.

Elser, J. J., Wu, C., González, A. L., Shain, D. H., Smith, H. J., Sommaruga, R., Williamson, C. E., Brahney, J., Hotaling, S., Vanderwall, J., Yu, J., Aizen, V., Aizen, E., Battin, T. J., Camassa, R., Feng, X., Jiang, H., Lu, L., Qu, J. J., Ren, Z., Wen, J., Wen, L., Woods, H. A., Xiong, X., Xu, J., Yu, G., Harper, J. T., and Saros, J. E.: Key rules of life and the fading cryosphere: Impacts in alpine lakes and streams, Global Change Biology, 26, 6644–6656, https://doi.org/10.1111/gcb.15362, 2020.

770 Evans, S., Martiny, J. B. H., and Allison, S. D.: Effects of dispersal and selection on stochastic assembly in microbial communities, ISME J, 11, 176–185, https://doi.org/10.1038/ismej.2016.96, 2017.

Fasching, C., Ulseth, A. J., Schelker, J., Steniczka, G., and Battin, T. J.: Hydrology controls dissolved organic matter export and composition in an Alpine stream and its hyporheic zone, Limnology and Oceanography, 61, 558–571, https://doi.org/10.1002/lno.10232, 2016.

775 Felden, J., Möller, L., Schindler, U., Huber, R., Schumacher, S., Koppe, R., Diepenbroek, M., and Glöckner, F. O.: PANGAEA - Data Publisher for Earth & Environmental Science, Sci Data, 10, 347, https://doi.org/10.1038/s41597-023-02269-x, 2023.

Fellman, J. B., Hood, E., Raymond, P. A., Hudson, J., Bozeman, M., and Arimitsu, M.: Evidence for the assimilation of ancient glacier organic carbon in a proglacial stream food web, Limnology and Oceanography, 60, 1118–1128, https://doi.org/10.1002/lno.10088, 2015.

780 Fox J, Weisberg S (2019). An R Companion to Applied Regression, Third edition. Sage, Thousand Oaks CA. https://socialsciences.mcmaster.ca/jfox/Books/Companion/.

Guenet, B., Danger, M., Abbadie, L., and Lacroix, G.: Priming effect: bridging the gap between terrestrial and aquatic ecology, Ecology, 91, 2850–2861, https://doi.org/10.1890/09-1968.1, 2010.

Guo, X., Yan, Q., Wang, F., Wang, W., Zhang, Z., Liu, Y., and Liu, K.: Habitat-specific patterns of bacterial communities in
785 a glacier-fed lake on the Tibetan Plateau, FEMS Microbiol Ecol, 100, 10.1093/femsec/fiae018, 2024.

Hallbeck, L. and Pedersen, K.: The Family Gallionellaceae, in: The Prokaryotes: Alphaproteobacteria and Betaproteobacteria, edited by: Rosenberg, E., DeLong, E. F., Lory, S., Stackebrandt, E., and Thompson, F., Springer, Berlin, Heidelberg, 853–858, https://doi.org/10.1007/978-3-642-30197-1_398, 2014.

Helms, J. R., Stubbins, A., Ritchie, J. D., Minor, E. C., Kieber, D. J., and Mopper, K.: Absorption spectral slopes and slope
790 ratios as indicators of molecular weight, source, and photobleaching of chromophoric dissolved organic matter, Limnology and Oceanography, 53, 955–969, https://doi.org/10.4319/lo.2008.53.3.0955, 2008.

Hill, M. O.: Diversity and Evenness: A Unifying Notation and Its Consequences, Ecology, 54, 427–432, https://doi.org/10.2307/1934352, 1973.

795 Hinton, M. J., Schiff, S. L., and English, M. C.: significance of storms for the concentration and export of dissolved organic carbon from two Precambrian Shield catchments, Biogeochemistry, 1997.

Hinton, M. J., Schiff, S. L., and English, M. C.: Sources and flowpaths of dissolved organic carbon during storms in two forested watersheds of the Precambrian Shield, Biogeochemistry, 41, 175–197, https://doi.org/10.1023/A:1005903428956, 1998.

Hood, E., Fellman, J., Spencer, R. G. M., Hernes, P. J., Edwards, R., D'Amore, D., and Scott, D.: Glaciers as a source of
800 ancient and labile organic matter to the marine environment, Nature, 462, 1044–1047, https://doi.org/10.1038/nature08580, 2009.

Hood, E., Battin, T. J., Fellman, J., O'Neel, S., and Spencer, R. G. M.: Storage and release of organic carbon from glaciers and ice sheets, Nature Geosci, 8, 91–96, https://doi.org/10.1038/ngeo2331, 2015a.

Hood, E., Battin, T. J., Fellman, J., O'neel, S., and Spencer, R. G. M.: Storage and release of organic carbon from glaciers and
805 ice sheets, Nature Geoscience, 8, 91–96, https://doi.org/10.1038/ngeo2331, 2015b.

Hood, E., Fellman, J. B., and Spencer, R. G. M.: Glacier Loss Impacts Riverine Organic Carbon Transport to the Ocean, Geophys. Res. Lett., 47, https://doi.org/10.1029/2020GL089804, 2020.

Hotaling, S., Hood, E., and Hamilton, T. L.: Microbial ecology of mountain glacier ecosystems: biodiversity, ecological connections and implications of a warming climate, Environmental Microbiology, 19, 2935–2948,
810 https://doi.org/10.1111/1462-2920.13766, 2017.

Hotaling, S., Foley, M. E., Zeglin, L. H., Finn, D. S., Tronstad, L. M., Giersch, J. J., Muhlfeld, C. C., and Weisrock, D. W.: Microbial assemblages reflect environmental heterogeneity in alpine streams, Global Change Biology, 25, 2576–2590, https://doi.org/10.1111/gcb.14683, 2019.

Huguet, A., Vacher, L., Relexans, S., Saubusse, S., Froidefond, J.-M., and Parlanti, E.: Properties of Fluorescent Dissolved
815 Organic Matter in the Gironde Estuary, Organic Geochemistry, 40, 706–719, https://doi.org/10.1016/j.orggeochem.2009.03.002, 2008.

Judd, K. E., Crump, B. C., and Kling, G. W.: Variation in Dissolved Organic Matter Controls Bacterial Production and Community Composition, Ecology, 87, 2068–2079, https://doi.org/10.1890/0012-9658(2006)87[2068:VIDOMC]2.0.CO;2, 2006.

820 Karstens, L., Asquith, M., Davin, S., Fair, D., Gregory, W. T., Wolfe, A. J., Braun, J., and McWeeney, S.: Controlling for Contaminants in Low-Biomass 16S rRNA Gene Sequencing Experiments, mSystems, 4, e00290-19, https://doi.org/10.1128/mSystems.00290-19, 2019.

Kellerman, A. M., Hawkings, J. R., Wadham, J. L., Kohler, T. J., Stibal, M., Grater, E., Marshall, M., Hatton, J. E., Beaton, A., and Spencer, R. G. M.: Glacier Outflow Dissolved Organic Matter as a Window Into Seasonally Changing Carbon Sources:
825 Leverett Glacier, Greenland, Journal of Geophysical Research: Biogeosciences, 125, e2019JG005161, https://doi.org/10.1029/2019JG005161, 2020.

Kellerman, A. M., Vonk, J., McColaugh, S., Podgorski, D. C., van Winden, E., Hawkings, J. R., Johnston, S. E., Humayun, M., and Spencer, R. G. M.: Molecular Signatures of Glacial Dissolved Organic Matter From Svalbard and Greenland, Global Biogeochemical Cycles, 35, e2020GB006709, https://doi.org/10.1029/2020GB006709, 2021.

830 Kellogg, C. T. E. and Deming, J. W.: Particle-associated extracellular enzyme activity and bacterial community composition across the Canadian Arctic Ocean, FEMS Microbiology Ecology, 89, 360–375, https://doi.org/10.1111/1574-6941.12330, 2014.

Kohler, T. J., Vinšová, P., Falteisek, L., Žárský, J. D., Yde, J. C., Hatton, J. E., Hawkings, J. R., Lamarche-Gagnon, G., Hood, E., Cameron, K. A., and Stibal, M.: Patterns in Microbial Assemblages Exported From the Meltwater of Arctic and Sub-Arctic
835 Glaciers, Front Microbiol, 11, 669, 10.3389/fmicb.2020.00669, 2020.

Kujawinski, E. B.: The Impact of Microbial Metabolism on Marine Dissolved Organic Matter, Annu. Rev. Mar. Sci., 3, 567–599, https://doi.org/10.1146/annurev-marine-120308-081003, 2011.

Lafrenière, M. J. and Sharp, M. J.: The Concentration and Fluorescence of Dissolved Organic Carbon (DOC) in Glacial and Nonglacial Catchments: Interpreting Hydrological Flow Routing and DOC Sources, Arctic, Antarctic, and Alpine Research,
840 36, 156–165, https://doi.org/10.1657/1523-0430(2004)036[0156:TCAFOD]2.0.CO;2, 2004.

Legendre, P. and Gallagher, E. D.: Ecologically meaningful transformations for ordination of species data, Oecologia, 129, 271–280, https://doi.org/10.1007/s004420100716, 2001.

Leibold, M. A., Holyoak, M., Mouquet, N., Amarasekare, P., Chase, J. M., Hoopes, M. F., Holt, R. D., Shurin, J. B., Law, R., Tilman, D., Loreau, M., and Gonzalez, A.: The metacommunity concept: a framework for multi-scale community ecology,
845 Ecology Letters, 7, 601–613, https://doi.org/10.1111/j.1461-0248.2004.00608.x, 2004.

Lenth R (2024). emmeans: Estimated Marginal Means, aka Least-Squares Means. R package version 1.10.2.090003, https://rvlenth.github.io/emmeans/, https://rvlenth.github.io/emmeans/.

Liu, Y., Shen, L., Zeng, Y., Xing, T., Xu, B., and Wang, N.: Genomic Insights of Cryobacterium Isolated From Ice Core Reveal Genome Dynamics for Adaptation in Glacier, Frontiers in Microbiology, 11, 2020.

850 Mann, P. J., Spencer, R. G. M., Hernes, P. J., Six, J., Aiken, G. R., Tank, S. E., McClelland, J. W., Butler, K. D., Dyda, R. Y., and Holmes, R. M.: Pan-Arctic Trends in Terrestrial Dissolved Organic Matter from Optical Measurements, Frontiers in Earth Science, 4, 2016.

Marcus, W. A., Roberts, K., Harvey, L., and Tackman, G.: An Evaluation of Methods for Estimating Manning's n in Small Mountain Streams, Mountain Research and Development, 12, 227–239, https://doi.org/10.2307/3673667, 1992.

855 Margesin, R., Zacke, G., and Schinner, F.: Characterization of Heterotrophic Microorganisms in Alpine Glacier Cryoconite, Arctic, Antarctic, and Alpine Research, 34, 88–93, https://doi.org/10.1080/15230430.2002.12003472, 2002.

McCrimmon, D. O., Bizimis, M., Holland, A., and Ziolkowski, L. A.: Supraglacial microbes use young carbon and not aged cryoconite carbon, Organic Geochemistry, 118, 63–72, https://doi.org/10.1016/j.orggeochem.2017.12.002, 2018.

McKnight, D. M., Boyer, E. W., Westerhoff, P. K., Doran, P. T., Kulbe, T., and Andersen, D. T.: Spectrofluorometric
860 characterization of dissolved organic matter for indication of precursor organic material and aromaticity, Limnology and Oceanography, 46, 38–48, https://doi.org/10.4319/lo.2001.46.1.0038, 2001a.

McKnight, D. M., Boyer, E. W., Westerhoff, P. K., Doran, P. T., Kulbe, T., and Andersen, D. T.: Spectrofluorometric characterization of dissolved organic matter for indication of precursor organic material and aromaticity, Limnology and Oceanography, 46, 38–48, https://doi.org/10.4319/lo.2001.46.1.0038, 2001b.

865 Milner, A. M., Khamis, K., Battin, T. J., Brittain, J. E., Barrand, N. E., Füreder, L., Cauvy-Fraunié, S., Gíslason, G. M., Jacobsen, D., Hannah, D. M., Hodson, A. J., Hood, E., Lencioni, V., Ólafsson, J. S., Robinson, C. T., Tranter, M., and Brown, L. E.: Glacier shrinkage driving global changes in downstream systems, Proceedings of the National Academy of Sciences, 114, 9770–9778, https://doi.org/10.1073/pnas.1619807114, 2017.

Moran, M. A. and Zepp, R. G.: Role of photoreactions in the formation of biologically labile compounds from dissolved
870 organic matter, Limnology and Oceanography, 42, 1307–1316, https://doi.org/10.4319/lo.1997.42.6.1307, 1997.

Murphy, K. R., Stedmon, C. A., Graeber, D., and Bro, R.: Fluorescence spectroscopy and multi-way techniques. PARAFAC, Anal. Methods, 5, 6557–6566, https://doi.org/10.1039/C3AY41160E, 2013.

Murphy, K. R., Stedmon, C. A., Wenig, P., and Bro, R.: OpenFluor– an online spectral library of auto-fluorescence by organic compounds in the environment, Anal. Methods, 6, 658–661, https://doi.org/10.1039/C3AY41935E, 2014.

875 Musilova, M., Tranter, M., Wadham, J., Telling, J., Tedstone, A., and Anesio, A. M.: Microbially driven export of labile organic carbon from the Greenland ice sheet, Nature Geoscience, 10, 360–365, https://doi.org/10.1038/ngeo2920, 2017.

Nienow, P., Sharp, M., and Willis, I.: Seasonal changes in the morphology of the subglacial drainage system, Haut Glacier d'Arolla, Switzerland, Earth Surface Processes and Landforms, 23, 825–843, https://doi.org/10.1002/(SICI)1096-9837(199809)23:9<825::AID-ESP893>3.0.CO;2-2, 1998.

880 Nizam, S., Sen, I. S., Vinoj, V., Galy, V., Selby, D., Azam, M. F., Pandey, S. K., Creaser, R. A., Agarwal, A. K., Singh, A. P., and Bizimis, M.: Biomass-Derived Provenance Dominates Glacial Surface Organic Carbon in the Western Himalaya, Environ. Sci. Technol., 54, 8612–8621, https://doi.org/10.1021/acs.est.0c02710, 2020.

Oksanen, J.: Vegan: community ecology package. R package version 1.8-5, http://www. cran. r-project. org, 2007.

Ommanney, C. S. L.: HISTORY OF GLACIER INVESTIGATIONS IN CANADA, n.d.

885 Pain, A. J., Martin, J. B., Martin, E. E., Rahman, S., and Ackermann, P.: Differences in the Quantity and Quality of Organic Matter Exported From Greenlandic Glacial and Deglaciated Watersheds, Global Biogeochemical Cycles, 34, e2020GB006614, https://doi.org/10.1029/2020GB006614, 2020.

Pandit, S. N., Kolasa, J., and Cottenie, K.: Contrasts between habitat generalists and specialists: an empirical extension to the basic metacommunity framework, Ecology, 90, 2253–2262, https://doi.org/10.1890/08-0851.1, 2009.

890 Parada, A. E., Needham, D. M., and Fuhrman, J. A.: Every base matters: assessing small subunit rRNA primers for marine microbiomes with mock communities, time series and global field samples, Environmental Microbiology, 18, 1403–1414, https://doi.org/10.1111/1462-2920.13023, 2016a.

Parada, A. E., Needham, D. M., and Fuhrman, J. A.: Every base matters: assessing small subunit rRNA primers for marine microbiomes with mock communities, time series and global field samples, Environmental Microbiology, 18, 1403–1414,
895 https://doi.org/10.1111/1462-2920.13023, 2016b.

Patriarca, C., Sedano-Núñez, V. T., Garcia, S. L., Bergquist, J., Bertilsson, S., Sjöberg, P. J. R., Tranvik, L. J., and Hawkes, J. A.: Character and environmental lability of cyanobacteria-derived dissolved organic matter, Limnology and Oceanography, 66, 496–509, https://doi.org/10.1002/lno.11619, 2021.

Peres-Neto, P. R., Legendre, P., Dray, S., and Borcard, D.: Variation partitioning of species data matrices: Estimation and comparison of fractions, Ecology, 87, 2614-2625, https://doi.org/10.1890/0012-9658(2006)87[2614:VPOSDM]2.0.CO;2, 2006.

Pradhananga, D. and Pomeroy, J. W.: Recent hydrological response of glaciers in the Canadian Rockies to changing climate and glacier configuration, Hydrology and Earth System Sciences, 26, 2605–2616, https://doi.org/10.5194/hess-26-2605-2022, 2022.

Pucher, M., Wünsch, U., Weigelhofer, G., Murphy, K., Hein, T., and Graeber, D.: staRdom: Versatile Software for Analyzing Spectroscopic Data of Dissolved Organic Matter in R, Water, 11, 2366, https://doi.org/10.3390/w11112366, 2019.

Qiagan: Powerwater Sterivex kit manufacturer protocol, 2019.

R Core Team: R: A language and environment for statistical computing. R Foundation for Statistical Computing, Vienna, Austria, Online: https://www. r-project. org, 2022.

Ramette, A.: Multivariate analyses in microbial ecology, FEMS Microbiol Ecol, 62, 142–160, https://doi.org/10.1111/j.1574-6941.2007.00375.x, 2007.

Raymond, P. A. and Bauer, J. E.: Use of 14C and 13C natural abundances for evaluating riverine, estuarine, and coastal DOC and POC sources and cycling: a review and synthesis, Organic Geochemistry, 32, 469–485, https://doi.org/10.1016/S0146-6380(00)00190-X, 2001.

Serbu, J. A., St.Louis, V. L., Emmerton, C. A., Tank, S., Criscitiello, A. S., Bhatia, M. Cavaco, M. A., Christenson, C., Cooke, C., Drapeau, H., Enns, S. J. A., Flett, J., Holland, K. M., Lavallee-Whiffen, J., Ma, M., Muir, C., Poesch, M., Shin, J., & Silins, U. Physicochemical, particulate matter, temperature, and hydrological datasets collected from climate-threatened glacial river headwaters on the eastern slopes of the Canadian Rocky Mountains (2019-2021), PANGAEA, 2023

Serbu, J. A., St. Louis, V. L., Emmerton, C. A., Tank, S. E., Criscitiello, A. S., Silins, U., Bhatia, M. P., Cavaco, M. A., Christenson, C., Cooke, C. A., Drapeau, H. F., Enns, S. J. A., Flett, J. E., Holland, K. M., Lavallee-Whiffen, J., Ma, M., Muir, C. E., Poesch, M., and Shin, J.: A Comprehensive Biogeochemical Assessment of Climate-Threatened Glacial River Headwaters on the Eastern Slopes of the Canadian Rocky Mountains, Journal of Geophysical Research: Biogeosciences, 129, e2023JG007745, https://doi.org/10.1029/2023JG007745, 2024.

Shi, Z., Allison, S. D., He, Y., Levine, P. A., Hoyt, A. M., Beem-Miller, J., Zhu, Q., Wieder, W. R., Trumbore, S., and Randerson, J. T.: The age distribution of global soil carbon inferred from radiocarbon measurements, Nat. Geosci., 13, 555–559, https://doi.org/10.1038/s41561-020-0596-z, 2020.

Singer, G. A., Fasching, C., Wilhelm, L., Niggemann, J., Steier, P., Dittmar, T., and Battin, T. J.: Biogeochemically diverse organic matter in Alpine glaciers and its downstream fate, Nature Geosci, 5, 710–714, https://doi.org/10.1038/ngeo1581, 2012.

Smith, H. J., Foster, R. A., McKnight, D. M., Lisle, J. T., Littmann, S., Kuypers, M. M. M., and Foreman, C. M.: Microbial formation of labile organic carbon in Antarctic glacial environments, Nature Geosci, 10, 356–359, https://doi.org/10.1038/ngeo2925, 2017.

Spencer, R. G. M., Guo, W., Raymond, P. A., Dittmar, T., Hood, E., Fellman, J., and Stubbins, A.: Source and biolability of ancient dissolved organic matter in glacier and lake ecosystems on the Tibetan Plateau, Geochimica et Cosmochimica Acta, 142, 64–74, https://doi.org/10.1016/j.gca.2014.08.006, 2014.

Spencer, R. G. M., Vermilyea, A., Fellman, J., Raymond, P., Stubbins, A., Scott, D., and Hood, E.: Seasonal variability of organic matter composition in an Alaskan glacier outflow: insights into glacier carbon sources, Environmental Research Letters, 9, 055005, 10.1088/1748-9326/9/5/055005, 2014.

Stevens, I. T., Irvine-Fynn, T. D. L., Edwards, A., Mitchell, A. C., Cook, J. M., Porter, P. R., Holt, T. O., Huss, M., Fettweis, X., Moorman, B. J., Sattler, B., and Hodson, A. J.: Spatially consistent microbial biomass and future cellular carbon release from melting Northern Hemisphere glacier surfaces, Commun Earth Environ, 3, 1–10, https://doi.org/10.1038/s43247-022-00609-0, 2022.

Stibal, M., Šabacká, M., and Žárský, J.: Biological processes on glacier and ice sheet surfaces, Nature Geoscience, https://doi.org/10.1038/ngeo1611, 2012a.

Stibal, M., Šabacká, M., and Žárský, J.: Biological processes on glacier and ice sheet surfaces, Nature Geosci, 5, 771–774, https://doi.org/10.1038/ngeo1611, 2012b.

Stubbins, A., Hood, E., Raymond, P. A., Aiken, G. R., Sleighter, R. L., Hernes, P. J., Butman, D., Hatcher, P. G., Striegl, R. G., Schuster, P., Abdulla, H. A. N., Vermilyea, A. W., Scott, D. T., and Spencer, R. G. M.: Anthropogenic aerosols as a source of ancient dissolved organic matter in glaciers, Nature Geoscience, 5, 198–201, https://doi.org/10.1038/ngeo1403, 2012a.

Stubbins, A., Hood, E., Raymond, P. A., Aiken, G. R., Sleighter, R. L., Hernes, P. J., Butman, D., Hatcher, P. G., Striegl, R. G., Schuster, P., Abdulla, H. A. N., Vermilyea, A. W., Scott, D. T., and Spencer, R. G. M.: Anthropogenic aerosols as a source of ancient dissolved organic matter in glaciers, Nature Geosci, 5, 198–201, https://doi.org/10.1038/ngeo1403, 2012b.

Tamames, J., Abellán, J. J., Pignatelli, M., Camacho, A., and Moya, A.: Environmental distribution of prokaryotic taxa, BMC Microbiology, 10, 85, https://doi.org/10.1186/1471-2180-10-85, 2010.

Tanentzap, A. J., Szkokan-Emilson, E. J., Kielstra, B. W., Arts, M. T., Yan, N. D., and Gunn, J. M.: Forests fuel fish growth in freshwater deltas, Nat Commun, 5, 4077, https://doi.org/10.1038/ncomms5077, 2014.

Tennant, C. and Menounos, B.: Glacier change of the Columbia Icefield, Canadian Rocky Mountains, 1919–2009, J. Glaciol., 59, 671–686, https://doi.org/10.3189/2013JoG12J135, 2013.

Tonkin, J. D., Altermatt, F., Finn, D. S., Heino, J., Olden, J. D., Pauls, S. U., and Lytle, David. A.: The role of dispersal in river network metacommunities: Patterns, processes, and pathways, Freshw Biol, 63, 141–163, https://doi.org/10.1111/fwb.13037, 2018.

Wadham, J. L., Hawkings, J. R., Tarasov, L., Gregoire, L. J., Spencer, R. G. M., Gutjahr, M., Ridgwell, A., and Kohfeld, K. E.: Ice sheets matter for the global carbon cycle, Nature Communications, 10, https://doi.org/10.1038/s41467-019-11394-4, 2019.

Weishaar, J. L., Aiken, G. R., Bergamaschi, B. A., Fram, M. S., Fujii, R., and Mopper, K.: Evaluation of Specific Ultraviolet Absorbance as an Indicator of the Chemical Composition and Reactivity of Dissolved Organic Carbon, Environ. Sci. Technol., 37, 4702–4708, https://doi.org/10.1021/es030360x, 2003.

30

Whiteside, J. H., Olsen, P. E., Eglinton, T. I., Cornet, B., McDonald, N. G., and Huber, P.: Pangean great lake paleoecology on the cusp of the end-Triassic extinction, Palaeogeography, Palaeoclimatology, Palaeoecology, 301, 1–17, https://doi.org/10.1016/j.palaeo.2010.11.025, 2011.

Wickham, H.: ggplot2, Springer International Publishing, Cham, https://doi.org/10.1007/978-3-319-24277-4, 2016.

Wilhelm, L., Singer, G. A., Fasching, C., Battin, T. J., and Besemer, K.: Microbial biodiversity in glacier-fed streams, ISME J, 7, 1651–1660, https://doi.org/10.1038/ismej.2013.44, 2013.

Zeglin, L. H.: Stream microbial diversity in response to environmental changes: review and synthesis of existing research, Frontiers in Microbiology, 6, 2015.

Zemp, M., Frey, H., Gärtner-Roer, I., Nussbaumer, S. U., Hoelzle, M., Paul, F., Haeberli, W., Denzinger, F., Ahlstrøm, A. P., Anderson, B., Bajracharya, S., Baroni, C., Braun, L. N., Cáceres, B. E., Casassa, G., Cobos, G., Dávila, L. R., Granados, H. D., Demuth, M. N., Espizua, L., Fischer, A., Fujita, K., Gadek, B., Ghazanfar, A., Hagen, J. O., Holmlund, P., Karimi, N., Li, Z., Pelto, M., Pitte, P., Popovnin, V. V., Portocarrero, C. A., Prinz, R., Sangewar, C. V., Severskiy, I., Sigurđsson, O., Soruco, A., Usubaliev, R., and Vincent, C.: Historically unprecedented global glacier decline in the early 21st century, Journal of Glaciology, 61, 745–762, https://doi.org/10.3189/2015JoG15J017, 2015.

Zhang, Y., Kang, S., Li, G., Gao, T., Chen, P., Li, X., Liu, Y., Hu, Z., Sun, S., Guo, J., Wang, K., Chen, X., and Sillanpää, M.: Dissolved organic carbon in glaciers of the southeastern Tibetan Plateau: Insights into concentrations and possible sources, PLOS ONE, 13, e0205414, https://doi.org/10.1371/journal.pone.0205414, 2018.

Zheng, Q., Lu, J., Wang, Y., and Jiao, N.: Genomic reconstructions and potential metabolic strategies of generalist and specialist heterotrophic bacteria associated with an estuary Synechococcus culture, FEMS Microbiol Ecol, 95, fiz017, https://doi.org/10.1093/femsec/fiz017, 2019.

Zhou, L., Zhou, Y., Hu, Y., Cai, J., Liu, X., Bai, C., Tang, X., Zhang, Y., Jang, K.-S., Spencer, R. G. M., and Jeppesen, E.: Microbial production and consumption of dissolved organic matter in glacial ecosystems on the Tibetan Plateau, Water Research, 160, 18–28, https://doi.org/10.1016/j.watres.2019.05.048, 2019a.

Zhou, Y., Zhou, L., He, X., Jang, K.-S., Yao, X., Hu, Y., Zhang, Y., Li, X., Spencer, R. G. M., Brookes, J. D., and Jeppesen, E.: Variability in Dissolved Organic Matter Composition and Biolability across Gradients of Glacial Coverage and Distance from Glacial Terminus on the Tibetan Plateau, Environ. Sci. Technol., 53, 12207–12217, https://doi.org/10.1021/acs.est.9b03348, 2019b.
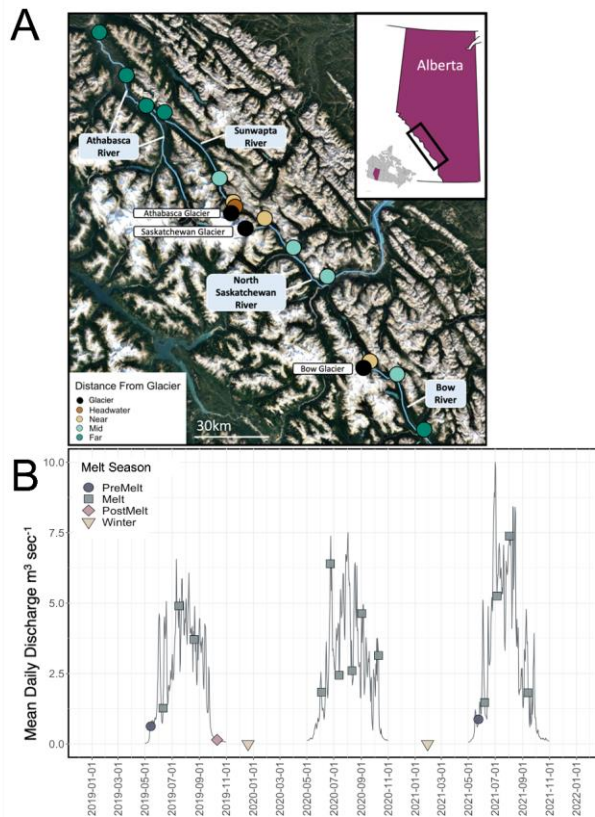
Figure 1: (A) Sampling locations of study sites on the Bow, North Saskatchewan, Sunwapta, and Athabasca Rivers, in Alberta, Canada (Google Earth © 2022). Locations are coloured by distance range, binned as headwater (0.2 km downstream), near (3-6 km downstream), mid (16-50 km downstream) and far (>50 km downstream). The inset map shows the location of the sampling region (black box) within Alberta. (B) Hydrograph of open-water discharge measured at the gauging station 3 km downstream of Athabasca glacier (station 07AA007, maintained by Environment and Climate Change Canada) from 2019–2021; note that data are not collected November-May. The location of the hydrologic station corresponds to the Sunwapta "near" site. Sample collection dates are demarcated, with corresponding melt season indicated.

Commented [TS1]: New figure uploaded.

15
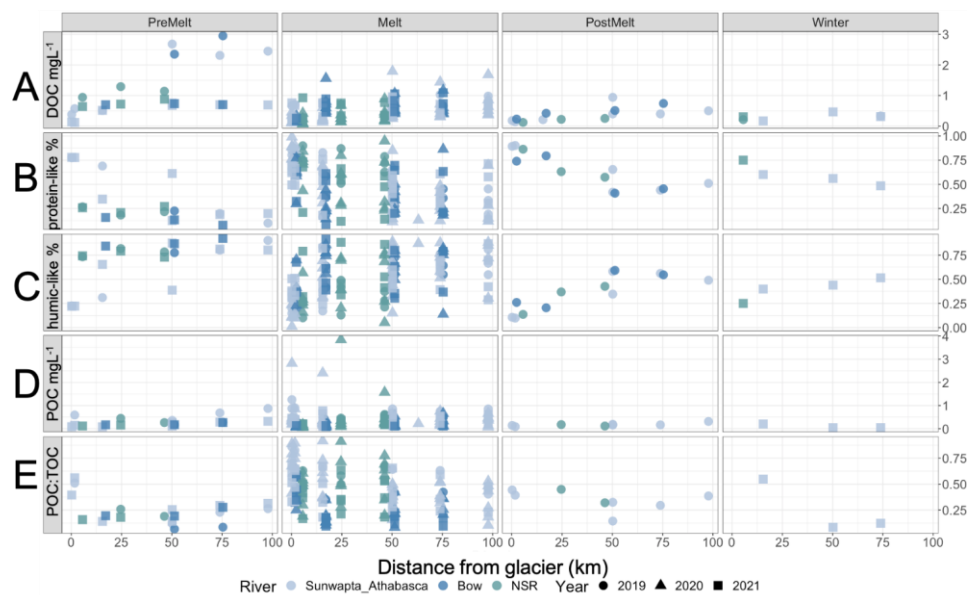
Figure 2: Plots of: (aA) DOC concentration, in mg L⁻¹ (bB) relative percentage (%) of protein-like DOM (eC) relative percentage (%) of humic-like DOM (dD); POC concentration in mg L⁻¹; and (eE) the ratio of POC to TOC (POC + DOC). Data are split by melt season and plotted against distance downstream, with river and year indicated.

2

25
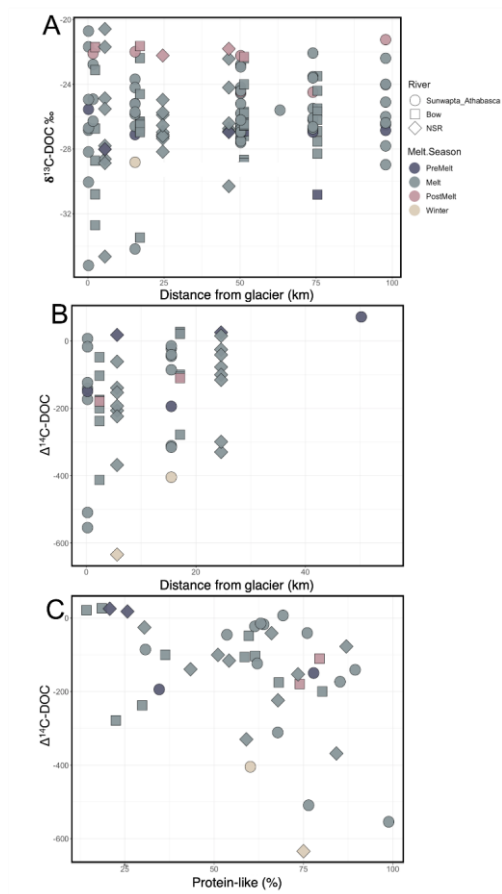
Figure 3: Plots of (A) s~~S~~tream δ^{13}C-DOC as a function of increasing distance from glacier terminus, (B) stream Δ^{14}C-DOC as a function of increasing distance from glacier terminus, and (C) the relationship between stream Δ^{14}C-DOC and the relative percentage of protein-like DOM (%). River and melt season are indicated by point shape and shading, respectively. Statistics for the relationships in (A) and (B) are provided in Table S4. A linear model of the relationship between Δ^{14}C-DOC and protein like DOM shows a significant negative slope (slope = -3.037; $R2_{adj}$ = 0.17, $F_{1,39}$ = 8.212, p = 0.007).

35
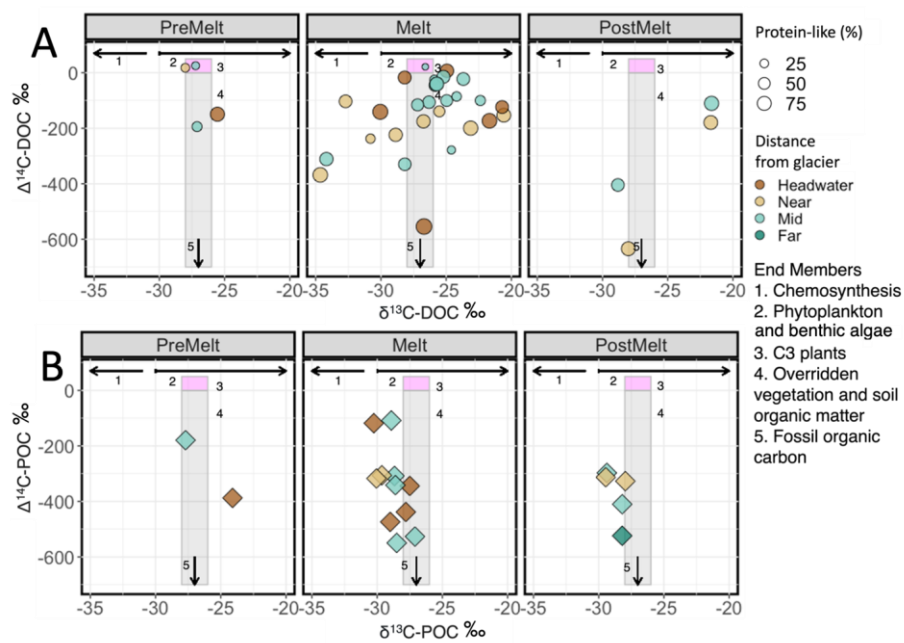
Figure 4: $\Delta^{14}C$ versus $\delta^{13}C$ values for (A) dissolved OC and (B) particulate OC, for all sites and seasons combined. In panel A, symbol size indicates the percentage protein-like DOM in each sample. Symbol size variation is not applicable in panel B. Different colours represent distance ranges. Numbered (1–5) pink and grey boxes and black lines represent literature isotopic ranges for various endmembers: (1) right arrow; (2) right arrow; (3) pink box; (4) grey box; (5) downwards arrow (Table S8).

4
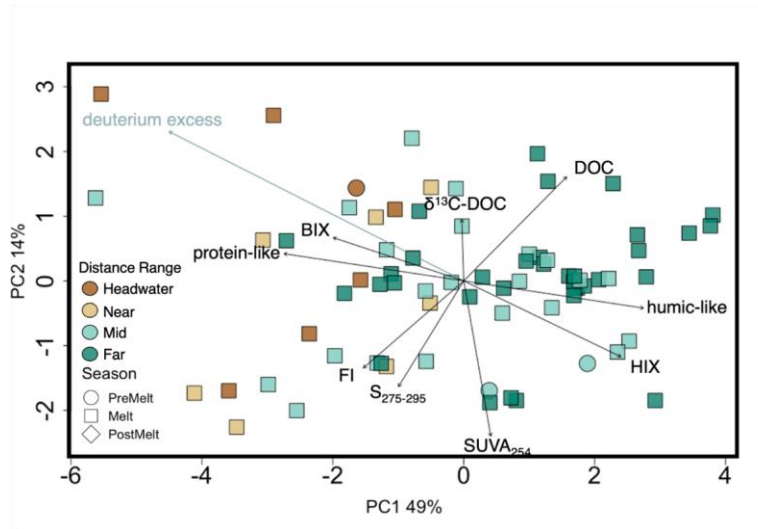
Figure 65: Principal component analysis of dissolved OM parameters (DOC concentration, $\delta^{13}C$-DOC, $S_{275-295}$, $SUVA_{254}$, BIX, FI, HIX, protein-like DOM, and humic-like DOM). Deuterium excess (blue text) is a passive overlay. Colours represent distance range, and shapes represent hydrological period. Percentages along the axes are explained variance.
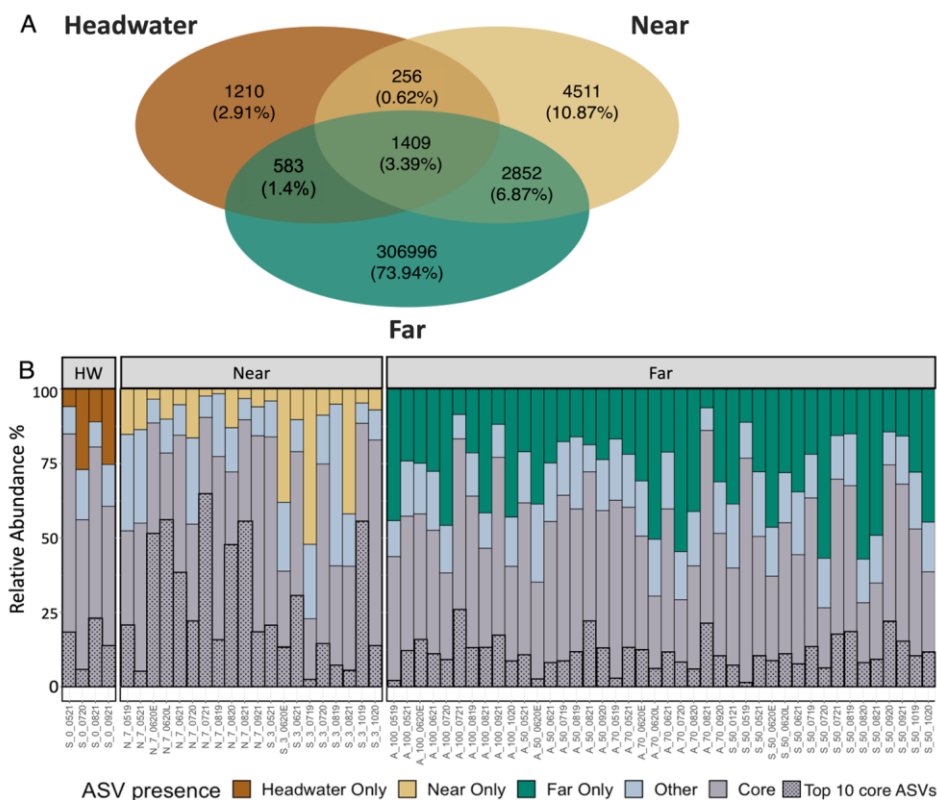
50

55

5

60

Figure 76: (A) Venn diagram showing the number of identified ASVs at the headwater (n = 4 samples), near (n = 20) and far sites (n = 42). (B) Bar plot showing the relative abundance of ASVs that are unique to each distance range, those ASVs identified in all three (headwater, near, far) distance bins ("core") or those that are shared between two distance bins ("other") in each sample. Sample abbreviations on the x-axis indicates river (Sunwapta (S), North Saskatchewan (N), Athabasca (A)), distance downstream (km), and sample date (as mmyy); suffixes "E" and "L" correspond to samples early, and late, in the associated sample month.
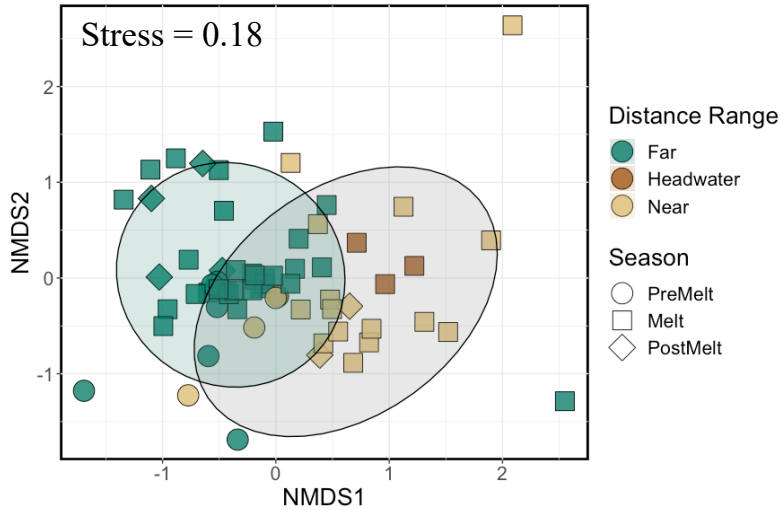
Figure 8̶7: NMDS of microbial assemblage composition across sites and sample dates. Shapes represent different hydrological periods while colour indicates distance range. Shaded circles represent the 95% confidence interval for significantly different groupings, where the far sites (green) were significantly different from headwater and near sites (brown and tan; pairwise perMANOVA p < 0.001 (h̶o̶l̶m̶s̶ Holms adjusted), R^2 = 0.09). Headwater and near sites were not significantly different from one another. S̶e̶e̶ Table S7 f̶o̶r̶ shows statistical comparisons; plots separated by year and river are shown in Fig. S7.
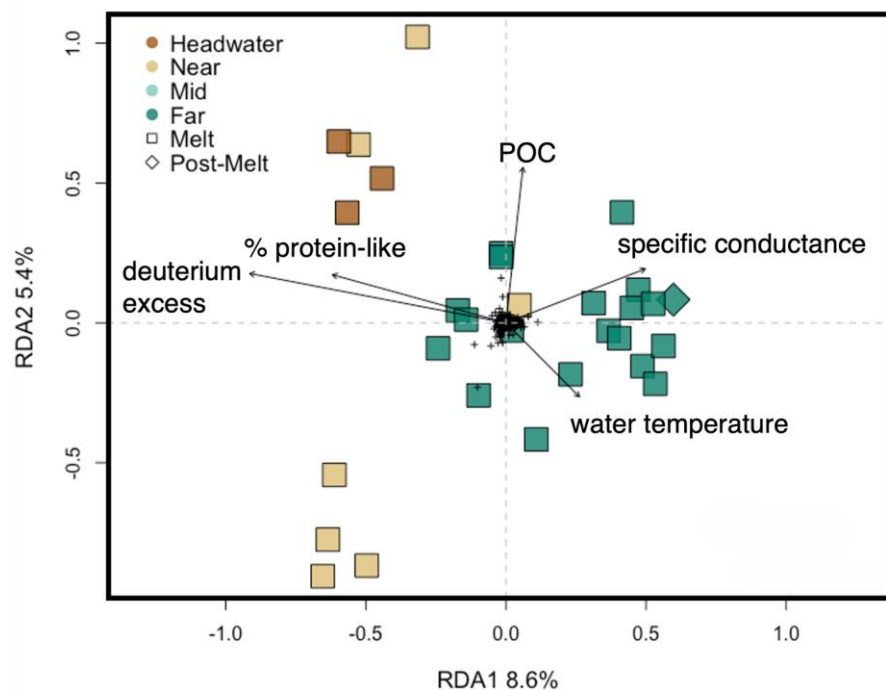
Figure 98: Redundancy analysis of microbial assemblage structure at the headwater, near, and far sites constrained by environmental variables, with black arrows showing significant explanatory variables as determined by a backward selection analysis (see methods). The percent variance explained by the first two RDA axes is shown on the axis labels. The full RDA has an adjusted R2 of 0.09, and unadjusted R2 of 0.25. Colours represent distance range and shapes represent hydrological period. Black crosses in the centre represent individual ASV scores.
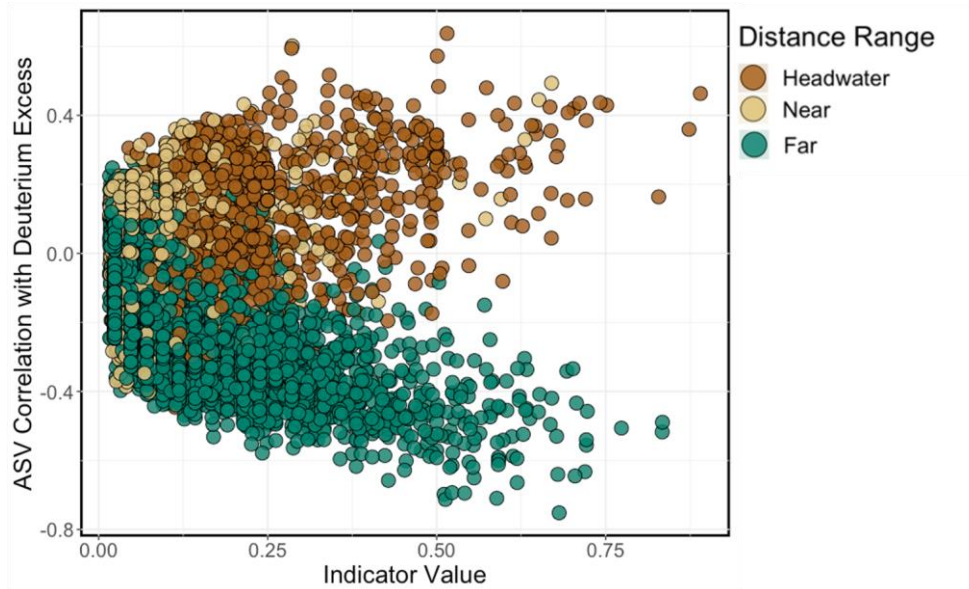
Figure ~~10~~9: A scatterplot of the relationship between the Spearman's rank correlation coefficient (ρ) for ASV relative abundance and deuterium excess, and ASV indicator species value. Brown, beige, and green circles represent the ASVs resolved in the headwater, near and far samples, respectively.